Optimal Aeroassisted Orbital Transfer with Predictive Time-Linear Control and Adaptation

A Thesis Submitted
in Partial Fulfillment of the Requirements
for the Degree of

Master of Technology

by

Praneeth Reddy Sudalagunta

under the Guidance of

Prof.Ashish Tewari

to the

Department of Aerospace Engineering
Indian Institute of Technology Kanpur

May, 2012

Certificate

It is certified that the work contained in the thesis titled, **"Optimal Aeroassisted Orbital Transfer with Predictive Time-Linear Control and Adaptation"**, by **Praneeth Reddy Sudalagunta**, has been carried out under my supervision and that this work has not been submitted elsewhere for the award of a degree.

Date: 4/5/2012

ProfessorAshish Tewari
Department of Aerospace Engineering
IIT Kanpur- 208016, India

To

My Parents Love,

Friendship

and

all that I believe to be true.

Acknowledgements

I would like to convey my heartfelt thanks and sincere gratitude to my thesis supervisor, **Prof. Ashish Tewari**, for his endless support and constant motivation for the past two years. Apart from being an incredible source of knowledge, he spent a considerable amount of his valuable time which gave me good exposure to the subject. Our frequent discussions helped me understand the problem at hand better and steered me in the right direction which led me this far. I am deeply grateful for all the encouragement he has given me. I would also like to thank **Prof. A.K.Ghosh**, **Prof. Ramprasad Potluri** and **Prof. Santosh Kumar Gupta** who have taught me important courses which helped me understand my work better and carry out quality research in my field.

I will forever be indebted to my loving and caring parents for their endless support and encouragement they have given me over the years.

Praneeth Reddy Sudalagunta

Abstract

This thesis presents optimal trajectory planning for an aeroassisted orbital transfer vehicle executing a co-planar maneuver from a circular high earth orbit to a circular low earth orbit, where only that part of the trajectory carried out within the earth's atmosphere is considered for optimization. The optimal trajectory is obtained for minimal control effort with fixed terminal time while satisfying the desired boundary conditions by developing the optimization problem into a nonlinear two-point boundary value problem. Numerical results are compared with those of an approximate optimal, free terminal time scheme and observed to have a significant reduction in the magnitude of the maximum control input, control power, and maximum heating rate. Apart from the above advantages, it is also observed that the optimal control law obtained for the given boundary conditions is linear in time, making it easier to implement. A closed-form approximation is developed for the states of the vehicle, when the control law is linear in time. A two-point boundary value problem which satisfies the desired boundary conditions for perturbed initial conditions with a time-linear control input is obtained and solved for the initial control input, the rate of change of the control input with respect to time and the terminal time. This solution is compared to that of the optimal control law for the new terminal time and is

observed that the latter oscillates about the former making the total control effort approximately equal which indicates that the predictive time-linear control law for the perturbed initial condition is an approximate optimal solution. The above methodology is compared with a fixed terminal-time LQR tracking system and the time-linear control law is observed to offer significant savings in terms of the total control effort along with providing an easily implementable predictive time-linear control law. In order to compensate for the uncertainty involved in estimating the parasite drag coefficient, an adaptive control system is implemented and shown to exhibit satisfactory performance.

Contents

List of Figures

List of Tables

Nomenclature

A	State jacobian matrix of plant
B	Control jacobian matrix of plant
C_{D_0}	Parasite drag coefficient
D	Drag
g	Acceleration due to gravity for Earth (9.81 m/s^2)
h	Geometric altitude
H	Scale height
$\mathbb{H}$	Hamiltonian
J	Objective function
K	Ballistic parameter
L	Lift
$\mathbb{L}$	Lagrangian
m	Mass of the spacecraft
r	Radius
P	Coefficient matrix for the Lyapunov function
Q	State weighting matrix
R	Control weighting matrix
R_e	Radius of Earth (6378.1 km)
S	Aerodynamic reference area

T	Thrust
t	Time
u	Normal acceleration or control input
δu	Control input to track the desired trajectory
V	Terminal weighting matrix
v	Velocity measured in Earth centered inertial frame
$\mathbf{x}$	State variable vector
δx	Deviation of the state variable
γ	Flight path angle
Δ	Error due to uncertainty in ballistic parameter
δ	Latitude, positive above the equator
η	Proportional design constant in the adaptive control law
Θ	Adaptive gain vector
$\boldsymbol{\lambda}$	Co-state variable vector, $\{\lambda_r,\ \lambda_v,\ \lambda_\gamma\}^T$
ρ	Density of atmosphere at a given altitude
Φ	Adaptation constant in the Lyapunov function
κ	Gain constant for the robust controller
Ψ	Differential design constant in the adaptive control law

Subscript

0	Initial condition

f	Final condition
h	Pertaining to the altitude of the AOT vehicle
m	Model
r	Pertaining to the state variable r
v	Pertaining to the state variable v
γ	Pertaining to the state variable γ

Superscript

$*$	Non-dimensional value
$'$	Pertaining to the perturbed case

Abbreviations

AOT	Aeroassisted orbital transfer
2PBVP	Two-point boundary value problem
LQR	Linear, quadratic regulator
HEO	High Earth orbit
LEO	Low Earth orbit

1

Introduction

In the realm of spacecraft dynamics and control, the ability of a spacecraft to be able to be transferred from one orbit to another is considered a great boon. As the activity of putting a spacecraft into a specific orbit in itself is very expensive, one would prefer having the freedom of being able to take it from one orbit to another. Early efforts towards achieving orbital transfer included using a propulsive maneuver where the thrust of the spacecraft is used to change the direction and magnitude of its velocity vector. In reality, the thrust applied is only for a very brief period of time. Hence, it can be considered as an impulse. Orbital transfer can be implemented to achieve a change in angle of inclination, eccentricity and distance from periapsis of a spacecraft in a given orbit. If the initial and the desired final orbits intersect with each other, then it is possible to achieve the maneuver using only one impulse. In the case where they don't, one would require at the least two impulses to carry out the maneuver where the first one is called the de-orbit impulse and the second one is called the re-orbit impulse. Aeroassisted orbital transfer (AOT) originated from the idea of using the de-orbit impulse to dip a spacecraft into a planet's atmosphere and use the atmospheric forces to achieve the desired conditions at the exit so as to collectively reduce the expenditure involved in producing the de-orbit and re-orbit impulses. As expected, a typical spacecraft cannot sustain the aerothermodynamic loads involved during re-entry. At the same time, a re-entry vehicle is designed to sustain much higher loads than that experienced during an AOT maneuver which clearly indicates that AOT maneuver requires a specially designed vehicle called the aeroassisted orbital transfer Vehicle.

1.1 Classification of Aeroassisted Orbital Transfer

Aeroassisted orbital transfer is a rather general term used in multitude of contexts, essentially to describe the use of atmospheric forces to control the exit conditions. Aeroassist can be considered for any mission that requires a change in orbit and if the vehicle is in the vicinity of a planet with a significant atmosphere. This includes various types of missions and maneuvers, each of them are classified below:

1.1.1 Types of Missions

Every mission has a goal that defines the mission, classification based on the type of mission is in essence classification on the basis of the goal required to be achieved

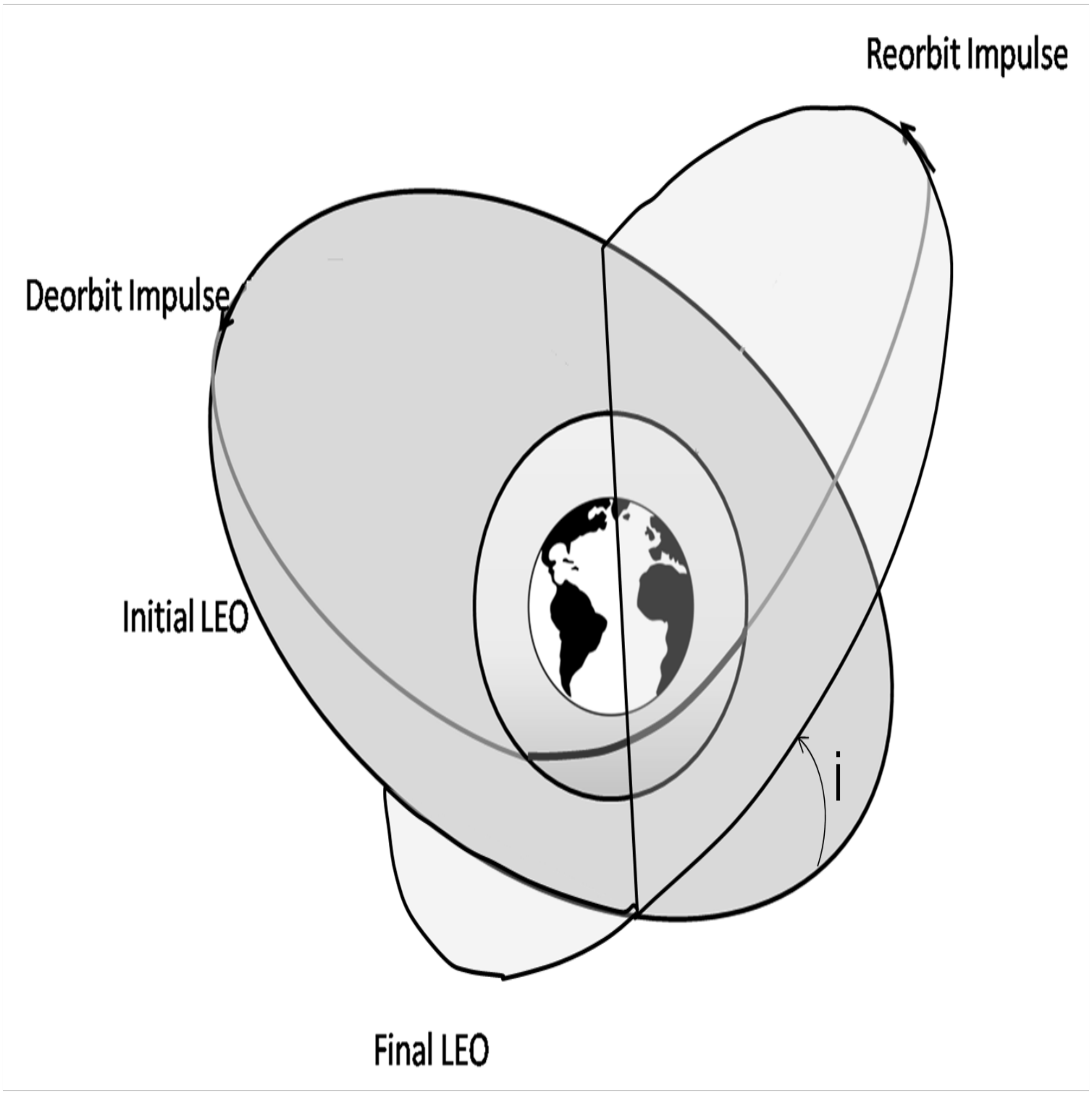

Figure 1.1: Plane Change Maneuver

pertaining to the change of orbit. Considering the fact that change of orbit includes various scenarios, the types of missions which are a candidate for using aeroassist are described below:

1.1.1.1 Plane Change Maneuver

Plane change maneuver is used essentially to change the inclination of the orbit, with no major change in the orbital altitude. In general, it is used to transfer the vehicle from one Low Earth Orbit (LEO) to another with significant change in the angle of inclination, occasionally as high as $60°$. The plane change is achieved by using a deorbit impulse from a LEO and dipping the vehicle into the atmosphere and then banking it to use the component of lift vector to facilitate the change in inclination. After the requisite inclination in plane is achieved, the vehicle is then put into another LEO by applying a deorbit impulse as described in Fig. 1.1. A typical vehicle used to carry out this maneuver is expected to be slender with a high Lift-Drag ratio and housing blended wing bodies with refractory metal thermal protection systems for reusability [1].

1.1.1.2 HEO-LEO Orbital Transfer

A HEO-LEO orbital transfer would typically require a transfer from a circular HEO to a circular LEO with no plane change required. A deorbit impulse is applied at the HEO to instantly reduce the velocity of the spacecraft, in order to decrease the perigee altitude of the elliptical transfer orbit. The perigee altitude should be small enough so

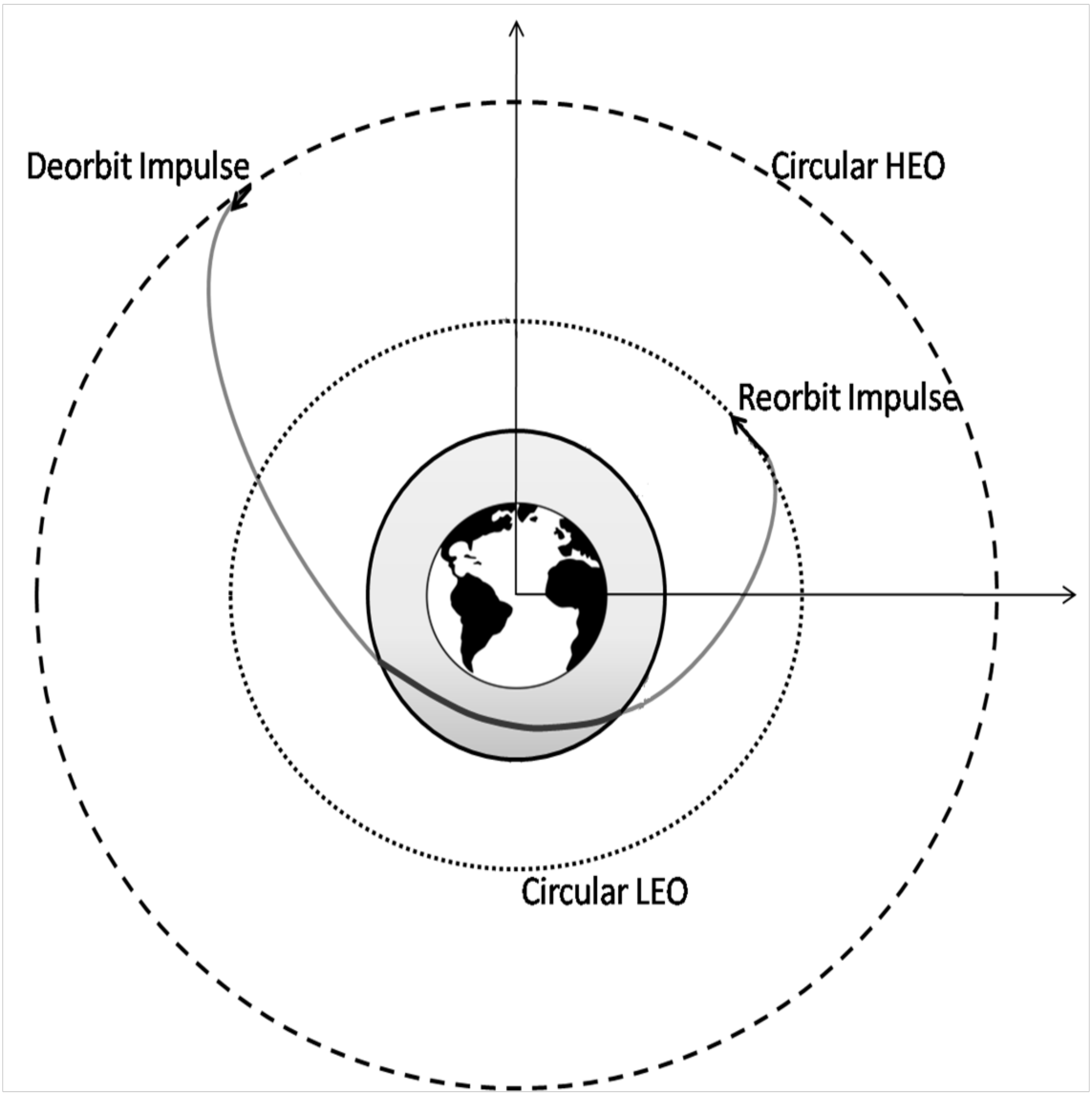

Figure 1.2: HEO-LEO Aeroassisted Orbital Transfer

that the spacecraft would reenter the Earth's atmosphere, use the aerodynamic drag to achieve a significant decrease in the length of the semi major axis. Then, another elliptical transfer orbit would be followed by the spacecraft after leaving the Earth's atmosphere with a reduced semi major axis and a reorbit impulse is applied at its apogee to put the spacecraft in to the desired circular LEO as shown in Fig. 1.2. The typical vehicle used to carry out such a mission is expected to be a cylindrical body with an ellipsoidal nose and a high lift-drag ratio. This vehicle is expected to experience high aerothermodynamic loading and might require a change in ablative shielding which would effect the operational utility of the vehicle [1]. Hence, there is an increasing need to reduce the aerothermodynamic loads on the vehicle. The present work considers this mission and emphasizes on reducing the control effort and heating rate.

1.1.1.3 Planetary Mission

Planetary missions are deep space missions from one planet to another where the entry trajectory is a hyperbolic one and the goal is to put the vehicle into a specific orbit around the planet, which is typically a circular or near circular orbit. A vehicle which is expected to carry out such missions is expected to have a circular cross section with a blunt spherical nose cone where the typical lift to drag ratios are lesser than that of the vehicles used in the other two missions. The emphasis for these missions is on using the atmosphere of the planet as a braking device to reduce the velocity of the vehicle. There are two types of missions under this category, namely

1. **Aerocapture:** As the entry trajectory from one planet to another is hyperbolic, the vehicle is allowed to enter into the planet's atmosphere, carry out a deep atmospheric pass to achieve the required velocity loss to put the vehicle into a low altitude circular orbit.

2. **Multipass Aerobraking:** During the approach from a hyperbolic entry trajectory, a considerably large propulsive force (retro rocket) is applied to achieved the requisite velocity loss to transfer the vehicle from the hyperbolic trajectory to a highly elliptical one. Then, a series of aerobraking passes are executed to slowly circularize the orbit until the vehicle falls into the desired orbit. Every atmospheric pass is followed by corrective rocket burns at apoapsis to ensure that the periapsis altitude is low enough to provide the requisite deceleration and high enough to avoid excess heating rate. Once the eccentricity of the the elliptical orbit approaches close to zero, a circularization impulse is applied to raise the periapsis altitude and put the spacecraft into the desired circular orbit as shown in Fig. 1.3.

1.1.2 Types of Maneuvers

AOT is classified based on the types of maneuvers that can be employed to achieve each of the above possible missions. Some of them are listed below:

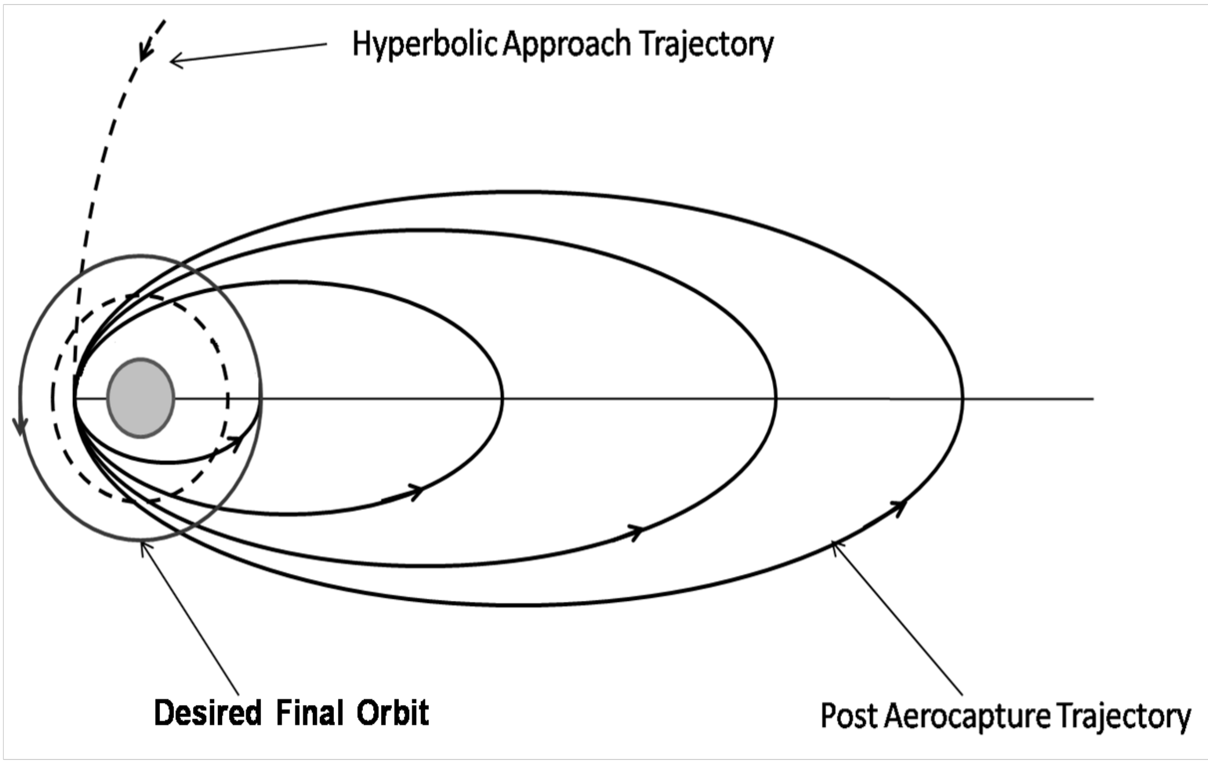

Figure 1.3: Aerocapture and Aerobraking

1.1.2.1 Aerogravity Assist

An aerogravity assist maneuver is carried out by an AOT vehicle where it dips into a planet's atmosphere, uses the lifting force to change the flight path angle and then uses the gravitational force of the planet to change its velocity. The present work uses aerogravity assist to carry out an orbital transfer.

1.1.2.2 Aerocruise

Aerocruise maneuver is typically used in synergetic plane change missions where the AOT vehicle dips into the atmosphere finds an altitude at which the drag would equal the thrust applied and uses the components of lift and gravity for plane change.

1.1.2.3 Aeroglide

Aeroglide, used for aerobraking and synergetic plane change missions, on the other hand does not involve any propulsive forces, instead glides into the atmosphere and uses appropriate control surfaces to achieve the required mission goal.

1.2 Review of Literature

The concept of utilizing a planet's atmosphere in order to achieve an orbital plane change as opposed to an all propulsive maneuver opened up a field called aeroassisted orbital transfer (AOT) which has led to active research in the past few decades [1]. The synergetic plane change maneuver that is essentially used in low Earth orbits (LEO) led to the development of an AOT maneuver from a high Earth orbit (HEO) to a LEO involving a significant decrease in the inertial speed. This is done by applying a deorbit impulse at the HEO and dipping the vehicle into the atmosphere, carrying out a pull-up maneuver where it uses the atmospheric drag to decelerate and then putting the vehicle into a LEO by applying a reorbit impulse at a given altitude. In certain cases, this maneuver might not include a considerable plane change, for such cases it is safe to assume planar motion [2]. The idea of aeroassisted orbital transfer was extended to planetary approach missions by introducing the concept of aerocapture where a hyperbolic planetary approach trajectory is converted into an elliptic orbit about the planet's center using the aerodynamic drag experienced by the spacecraft in the upper reaches of its atmosphere. The spacecraft can transfer from one orbit to another using aerobraking which essentially uses the concomitant atmospheric drag as an aerodynamic brake to shed excess velocity, in order to change the eccentricity of its orbit. Kumar and Tewari [3, 4] presented a strategy for trajectory and attitude simulation of a planetary approach mission to Mars and Earth respectively, where an aerocapture maneuver is followed by a series of aerobraking passes to achieve the desired near circular orbit taking the presence of storms and diurnal variations of the martian atmosphere into consideration.

The extent of deceleration required for these maneuvers raised important questions about the heating rate of the spacecraft. It was also observed that the rate of heat transfer to the spacecraft played a major role in deciding the performance of such a vehicle and in assessing the overall cost of the mission [5]. In order to fully exploit the advantages of an aeroassisted maneuver, it is important to minimize the control effort through optimization. Interesting research in the field of optimal aeroassisted orbital transfer with heating rate constraints was presented in [6, 7]. The former discusses the optimal trajectory for a synergetic plane change maneuver using steady aero cruise with heating rate path constraint and proved that the optimal thrust usage is sensitive to the heating rate limit chosen and emphasizes on the need to choose this value judiciously. Whereas, the latter describes that fuel-optimal strategies lead to higher heat transfer rate to the spacecraft, thus increasing the thermal protection mass which in turn could reduce fuel savings. Hence, emphasis was put on obtaining optimal trajectories with heating rate path constraints minimizing the propellant and the thermal protection mass.

The governing equations for reentry dynamics are nonlinear differential equations and do not generally have closed-form analytical solutions. Early efforts were made to obtain approximate closed-form analytical solutions which provided researchers an alternative over time consuming iterative numerical methods. Loh [8] presented a myriad of closed-form first order approximate analytical solutions for various reentry problems. The difference between the inertial and gravitational forces was assumed to be constant, which will be the case when aerodynamic forces dominate as they would during reentry. Beyond designing an optimal trajectory, it is important to consider the implementation of a feedback controller in order to ensure that the vehicle follows the desired path. Due to non-linearity of the solution of an optimal control problem, the implementation may not be straight forward. In the last two decades, the focus from designing better optimal trajectories has shifted to designing implementable and practically applicable near-optimal trajectories [9, 10]. It is also important to note that the easiest control algorithm to implement, apart from a constant control profile, is a linearly varying control profile with time using a simple timing (or clockwork) mechanism. Hence, a time-linear control profile is quite valuable if it can be demonstrated that such a control results in an optimal AOT. In such a case, there is no need to solve an online 2PBVP optimization problem for determining the nominal trajectory, which is typically required for other methods [9, 10, 11]. Mishne et al. [9] assumed that the aerodynamic force at reentry altitudes is much larger than the inertial and gravitational forces, expressed the feedback control law as a series expansion of the ratio of the atmospheric scale height to the radius of the earth and obtained zeroth order and first order solutions by truncating the series expansion to the first and second terms respectively. Whereas, Shen and Lu [11] emphasized on the need for onboard entry trajectory generation with inequality path constraints and terminal conditions precisely met. Though the computational effort is reduced by simplifying the complexity involved in satisfying the path constraints by using the bank angle obtained from the equilibrium glide condition at every instant of time, it still requires relatively high computational effort as it uses a linear time varying feedback control law. Naidu et al. [12], on the other hand, obtained a deterministic optimal trajectory for a given set of boundary conditions and acknowledged that initial conditions of the spacecraft at reentry can marginally deviate from the expected ones. In order to compensate for such deviations, they developed an optimum control guidance law which is a combination of the deterministic trajectory obtained and the trajectory obtained using a stochastic model for the linearized state equations. Though, each of the strategies used in these cases have their own merits, they do not result in an easily implementable time linear optimal control law. It would be ideal to obtain such a control law without compromising much on accuracy.

The present work deals with optimal trajectory planning for coplanar orbital transfer of an AOT vehicle from a HEO to a LEO. Such a maneuver would also include the deorbit and reorbit impulses which are not considered during optimization. The mathematical model for the reentry trajectory of an AOT vehicle is discussed, followed by the development of optimization problem, obtaining the Euler-Lagrange equations, boundary conditions and the optimal control law. This is followed by the development of the 2PBVP from the optimization problem and its numerical solution. The control profile obtained from the numerical solution was observed to be linear in time, an approximate closed-form solution of the state equations for a time linear control profile is derived. Additionally, a terminal-time tracker is designed to meet the exit conditions despite deviations in the initial conditions. An alternate method, hereafter referred as predictive time-linear control, is suggested. This method is a novel idea where the final time is changed to accommodate the deviations in initial state and the control law thus obtained is easily implementable due to its linearity in time. The results are compared to that of the terminal tracking system and are observed to involve smaller control effort in the case of predictive time-linear control. Additionally, an adaptive control system is designed to take into account the uncertainty in the coefficient of drag arising due to the change in angle of attack. It is observed that the adaptive control system satisfactorily meets the exit conditions despite the uncertainty in coefficient of drag.

2

Mathematical Model

Let us consider the motion of an AOT vehicle referenced to a non-rotating, spherical planet (Earth) at the boundary of its atmosphere. The motion is restricted to a plane formed by the radial vector and the line of apsides of the initial orbit (HEO). The state of the spacecraft completely describes the position and the rate of change of position at any instant of time on this plane. In order to describe the position of a body on such a plane, we would require two quantities; the radial distance of the vehicle from the center of the earth r and the latitude δ. Similarly, in order to describe the rate of change of position, we would require two more quantities; the velocity of the vehicle v and the angle made by the velocity vector with the local horizon frame called the flight path angle γ (by convention, the angle measured above the horizon is considered positive) as shown in Fig. 2.1. These four quantities completely describe the state of an AOT vehicle and its equations of motion provide us with the state equations (see

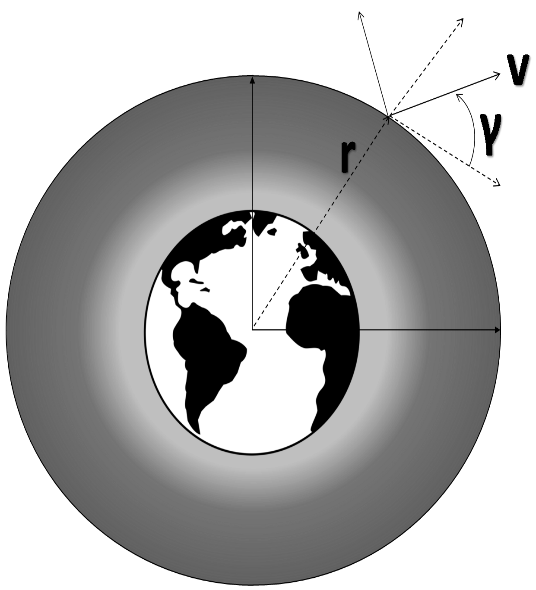

Figure 2.1: Co-ordinate axes at local horizon

[13]):

$$\frac{\mathrm{d}r}{\mathrm{dt}} = v\ \sin\gamma \tag{2.1}$$

$$r\frac{\mathrm{d}\delta}{\mathrm{dt}} = v\ \cos\gamma \tag{2.2}$$

$$m\frac{\mathrm{d}v}{\mathrm{dt}} = -mg\ \sin\gamma - D \tag{2.3}$$

$$mv\frac{\mathrm{d}\gamma}{\mathrm{dt}} = \frac{mv^2}{r}\ \cos\gamma - mg\ \cos\gamma + L \tag{2.4}$$

Equations (2.1) and (2.2) are the kinetic equations of motion and can be obtained from Fig. 2.1, while Eq. (2.3) and (2.4) are kinematic equations of motion which can be obtained from the free body diagram given in Fig.2.2. The latitude δ, though

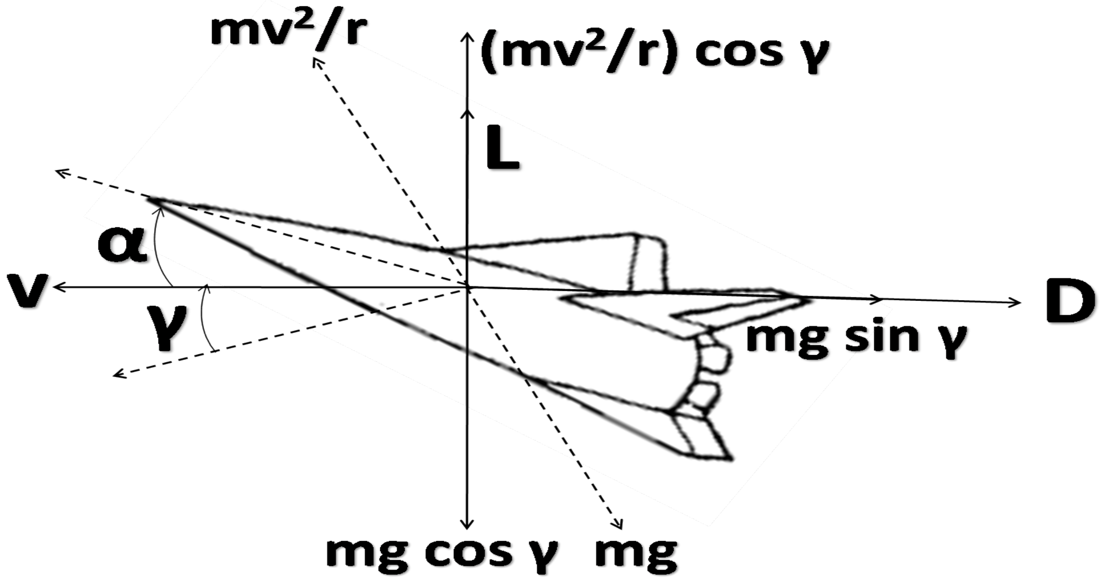

Figure 2.2: Free body diagram

dependent on the other state variables does not influence them in anyway. Hence, the equation for δ is excluded from the state equations. It is to be noted that L (force due to Lift) is the only control input in the state equations as the induced drag is neglected.

2.1 Assumptions:

1. Motion of the vehicle is restricted to a plane, as a typical AOT maneuver from a higher Earth circular orbit to a low Earth orbit does not include considerable plane change. Hence, it is valid to assume planar motion.

2. Effect of rotation of the planet on the vehicle is neglected, as the relative wind speed at a typical reentry altitude is equal to that of the spacecraft.

3. Acceleration due to gravity (g) is assumed to be constant, as the ratio of the maximum change in altitude during the maneuver to the radial distance from the center of the Earth is negligible.

4. Variation of density of the atmosphere with respect to altitude is assumed to be exponential and is given by (2.5). This assumption is valid at reentry altitudes and a comparison with standard atmosphere is given in [13].

$$\rho = \rho_s \mathrm{e}^{-h/H} \tag{2.5}$$

5. Only parasite drag accounts for the total drag, as the induced drag is small enough to be neglected and the expression for the drag co-efficient is given by (2.6).

$$C_D = C_{D_0} = \frac{D}{(1/2)\rho v^2 S} \tag{2.6}$$

2.2 State Equations

The state equations for the AOT vehicle can be written as follows:

$$\begin{Bmatrix} \dot{r} \\ \dot{v} \\ \dot{\gamma} \end{Bmatrix} = \begin{Bmatrix} v \sin\gamma \\ -g \sin\gamma - K\mathrm{e}^{-\frac{(r-R_e)}{H}} v^2 \\ (v/r - g/v) \cos\gamma + u/v \end{Bmatrix}; \tag{2.7}$$

$$K = \frac{\rho_s C_{D_0}}{2(m/S)} \tag{2.8}$$

$$u = L/m. \tag{2.9}$$

Tao et al. and Shen, Lu [10, 11] emphasize on the importance of constraining the heating rate, magnitude of aerodynamic forces and free stream dynamic pressure. The choice of $u \quad (L/m)$ as a control variable is ideal, as it has a one-to-one relationship with free stream dynamic pressure, magnitude of net aerodynamic force (which depends on dynamic pressure and C_L, the product of which is proportional to u) and the heating rate depends on the product of dynamic pressure and velocity. Hence, minimizing u would mean reducing all the above quantities, one way or the other. The AOT maneuver requires the vehicle to reach specific exit conditions, thus leading to a two-point boundary value problem (2PBVP).

3

Euler-Lagrange Formulation

An optimization problem can be described as obtaining a control law for a system of state equations while minimizing an objective function for a given set of initial conditions and final conditions, where the state equations give the trajectory followed by the vehicle for a given control law. The Euler-Lagrange equations are the necessary conditions for optimality which emerge from the fact that optimality is achieved at a stationary point. The solution of the Euler-Lagrange equations from t_0 to t_f gives us the stationary points of the system for which the given objective function is at its extrema throughout the interval.

Theorem. *Let $\mathbf{x} \in \mathbb{R}^3$ and $u \in \mathbb{R}$ represent the state space and the control space of a given system and the evolution of the states with respect to time be given by,*

$$\dot{\mathbf{x}} = \mathbf{f}(\mathbf{x}, u) \tag{3.1}$$

where $f : \mathbb{R}^3 \times \mathbb{R} \to \mathbb{R}^3$*. Let the objective function to be minimized be given by,*

$$J = \int_{t_0}^{t_f} \mathbb{L}(\mathbf{x}, u)dt \tag{3.2}$$

where $\mathbb{L} : \mathbb{R}^3 \times \mathbb{R} \to \mathbb{R}$ *represents the Lagrangian or cost function. Let the above minimization problem be constrained by the initial and final states of the system,* $\mathbf{x}(t_0)$ *and* $\mathbf{x}(t_f)$ *respectively, then the necessary conditions for minimization are given by the Euler-Lagrange Equations given below (see [14] and [15]):*

$$\dot{\mathbf{x}} = \left(\frac{\partial \mathbb{H}}{\partial \boldsymbol{\lambda}}\right)^T \tag{3.3}$$

$$\dot{\boldsymbol{\lambda}} = -\left(\frac{\partial \mathbb{H}}{\partial \mathbf{x}}\right)^T \tag{3.4}$$

$$\frac{\partial \mathbb{H}}{\partial u} = 0 \tag{3.5}$$

where,

$$\mathbb{H}(\mathbf{x}, u) = \mathbb{L}(\mathbf{x}, u) + \boldsymbol{\lambda}^T \mathbf{f}(\mathbf{x}, u) \tag{3.6}$$

is the Hamiltonian of the function with $\mathbb{H} : \mathbb{R}^3 \times \mathbb{R} \to \mathbb{R}$ *and* $\boldsymbol{\lambda} \in \mathbb{R}^3$*.*

Proof. *Consider the objective function, given in* (3.2)

$$J = \int_{t_0}^{t_f} \mathbb{L}(\mathbf{x}, u)dt \tag{3.7}$$

and adjoin the Lagrangian ($\mathbb{L}$) *with* (3.1) *using a vector of Lagrangian multipliers* $\boldsymbol{\lambda}$ *where* $\boldsymbol{\lambda} \in \mathbb{R}^3$

$$\bar{J} = \int_{t_0}^{t_f} (\mathbb{L}(\mathbf{x}, u) + \boldsymbol{\lambda}^T(\mathbf{f}(\mathbf{x}, u) - \dot{\mathbf{x}}))dt \tag{3.8}$$

$$\bar{J} = \int_{t_0}^{t_f} (\mathbb{L}(\mathbf{x}, u) + \boldsymbol{\lambda}^T\mathbf{f}(\mathbf{x}, u))dt - \int_{t_0}^{t_f} \boldsymbol{\lambda}^T\dot{\mathbf{x}}dt \tag{3.9}$$

Let,

$$\mathbb{H}(\mathbf{x}, u) = \mathbb{L}(\mathbf{x}, u) + \boldsymbol{\lambda}^T\mathbf{f}(\mathbf{x}, u) \tag{3.10}$$

where $\mathbb{H} : \mathbb{R}^3 \times \mathbb{R} \to \mathbb{R}$ *is called the Hamiltonian. Using* (3.10) *in* (3.9)*, we have*

$$\bar{J} = \int_{t_0}^{t_f} \mathbb{H}(\mathbf{x}, u)dt - \int_{t_0}^{t_f} \boldsymbol{\lambda}^T\dot{\mathbf{x}}dt \tag{3.11}$$

By using integration by parts on the second integral, we have

$$\bar{J} = -[\boldsymbol{\lambda}^T\mathbf{x}]_{t_0}^{t_f} + \int_{t_0}^{t_f} \mathbb{H}(\mathbf{x}, u)dt + \int_{t_0}^{t_f} \dot{\boldsymbol{\lambda}}^T\mathbf{x}dt \tag{3.12}$$

Using calculus of variations, considering a variation in $\bar{J}$ *due to variations in* u *and* $\mathbf{x}$ *for fixed times* t_0 *and* t_f *we have*

$$\delta\bar{J} = -(\boldsymbol{\lambda}^T\boldsymbol{\delta}\mathbf{x})_{t=t_f} + (\boldsymbol{\lambda}^T\boldsymbol{\delta}\mathbf{x})_{t=t_0} + \int_{t_0}^{t_f} \left(\left(\frac{\partial\mathbb{H}}{\partial\mathbf{x}} + \dot{\boldsymbol{\lambda}}^T\right)\boldsymbol{\delta}\mathbf{x} + \left(\frac{\partial\mathbb{H}}{\partial u}\right)\delta u\right)dt \tag{3.13}$$

Let,

$$\dot{\boldsymbol{\lambda}}^T = -\frac{\partial \mathbb{H}}{\partial \mathbf{x}} \tag{3.14}$$

$$\frac{\partial \mathbb{H}}{\partial u} = 0 \tag{3.15}$$

and considering the fact that the states of the system are fixed at t_0 *and* t_f*, we have*

$$\boldsymbol{\delta}\mathbf{x}(t_0) = \mathbf{0} \tag{3.16}$$

$$\boldsymbol{\delta}\mathbf{x}(t_f) = \mathbf{0} \tag{3.17}$$

Using (3.14)-(3.17) *in* (3.13)*, we have*

$$\delta \bar{J} = 0 \tag{3.18}$$

which is the necessary condition for optimality. Hence (3.14), (3.15) *along with the state equation* (3.1) *form the necessary conditions for optimality.*

The Euler-Lagrange equations (3.3)-(3.5) coupled with the boundary conditions, form a two-point boundary value problem which can be solved for u.

For the AOT vehicle under consideration (2.7) it is desired to carry out an orbital transfer from a HEO orbit to a LEO orbit where the vehicle reenters the atmosphere at a radius r_0, velocity v_0 and flight path angle γ_0. It is also expected to exit the atmosphere at a radius r_f, velocity v_f and flight path angle γ_f within time t_f. It is desired to minimize the control effort (u) of the spacecraft throughout the maneuver. For the given optimization problem, $\mathbf{x} = \{r \quad v \quad \gamma\}^T$, $\boldsymbol{\lambda} = \{\lambda_r \quad \lambda_v \quad \lambda_\gamma\}^T$, $\mathbf{x}(t_0) = \{r_0 \quad v_0 \quad \gamma_0\}$, $\mathbf{x}(t_f) = \{r_f \quad v_f \quad \gamma_f\}$, $\phi = 0$ and $\mathbb{L} = Ru^2$ where R is a positive real number. The co-state equations for this optimization problem are given by:

$$\dot{\boldsymbol{\lambda}} = \left\{ \begin{array}{c} -\lambda_v K \mathrm{e}^{-\left(\frac{r-R_e}{H}\right)} v^2/H + \lambda_\gamma v \ \cos\gamma/r^2 \\ -\lambda_r \ \sin\gamma + 2\lambda_v K \mathrm{e}^{-\left(\frac{r-R_e}{H}\right)} v - \lambda_\gamma \left((1/r + g/v^2) \ \cos\gamma - u/v^2\right) \\ -\lambda_r v \ \cos\gamma + \lambda_v g \ \cos\gamma + \lambda_\gamma \left((v/r - g/v) \ \sin\gamma\right) \end{array} \right\} \tag{3.19}$$

The optimal control law can be derived from (3.5) and is given by:

$$u = -\frac{\lambda_\gamma}{2Rv} \tag{3.20}$$

(3.20) can be substituted into (3.19) and (2.7) to obtain the following system of equations:

$$\left\{ \begin{array}{c} \dot{\mathbf{x}} \\ \dot{\boldsymbol{\lambda}} \end{array} \right\} = \left\{ \begin{array}{c} v \ \sin\gamma \\ -g \ \sin\gamma - K \mathrm{e}^{-\left(\frac{r-R_e}{H}\right)} v^2 \\ (v/r - g/v) \ \cos\gamma - \lambda_\gamma/2Rv^2 \\ -\lambda_v K \mathrm{e}^{-\left(\frac{r-R_e}{H}\right)} v^2/H + \lambda_\gamma v \ \cos\gamma/r^2 \\ -\lambda_r \sin\gamma + 2\lambda_v K \mathrm{e}^{-\left(\frac{r-R_e}{H}\right)} v - \lambda_\gamma \left((1/r + g/v^2) \ \cos\gamma + \lambda_\gamma/2Rv^3\right) \\ -\lambda_r v \ \cos\gamma + \lambda_v g \ \cos\gamma + \lambda_\gamma \left((v/r - g/v) \ \sin\gamma\right) \end{array} \right\} \tag{3.21}$$

The boundary conditions describe the state of the system (AOT vehicle) either completely or partially at t_0 and t_f. The de-orbit impulse applied at the initial orbit (HEO) decides the state of the system at t_0 and is assumed to be known. As discussed in [9], for such a maneuver typical initial altitude lies between $70 - 100km$, initial velocity lies between $8 - 10km/sec$ and the reentry flight path angle is not more than a few degrees (pointing downwards or negative). The boundary conditions are given by:

$$\mathbf{x}(t_0) = \left\{ \begin{array}{c} r_0 \\ \\ v_0 \\ \\ \gamma_0 \end{array} \right\}; \qquad \mathbf{x}(t_f) = \left\{ \begin{array}{c} r_f \\ \\ v_f \\ \\ \gamma_f \end{array} \right\}; \tag{3.22}$$

Equations (3.21) and (3.22) form a two-point boundary value problem (2PBVP) which does not have a closed form analytical solution and hence a numerical method has to be used in order to obtain u .

4

Optimal Trajectory Solution

4.1 Solution of 2PBVP

Equations (3.21) and (3.22) are solved using a collocation method by dividing the entire interval into several sub-intervals by setting up collocation points, and approximating solution in each sub-interval by a cubic spline collocated at the mid-point. The collocated polynomials are substituted in the continuous-time differential equations to convert them into a system of difference equations which when used along with the boundary conditions and solved for coefficients of the cubic splines, result in the solution of the 2PBVP [16]. The results are presented in Fig 4.1 and compared with the solution obtained in [9] for the case of pull-up maneuver using data of Table 4.1.

Mishne et al. [9], as described in the Introduction, obtains an approximate optimal guidance law for an AOT vehicle executing a planar orbital transfer maneuver. The reentry conditions used in [9] and in the present case are similar except for the final

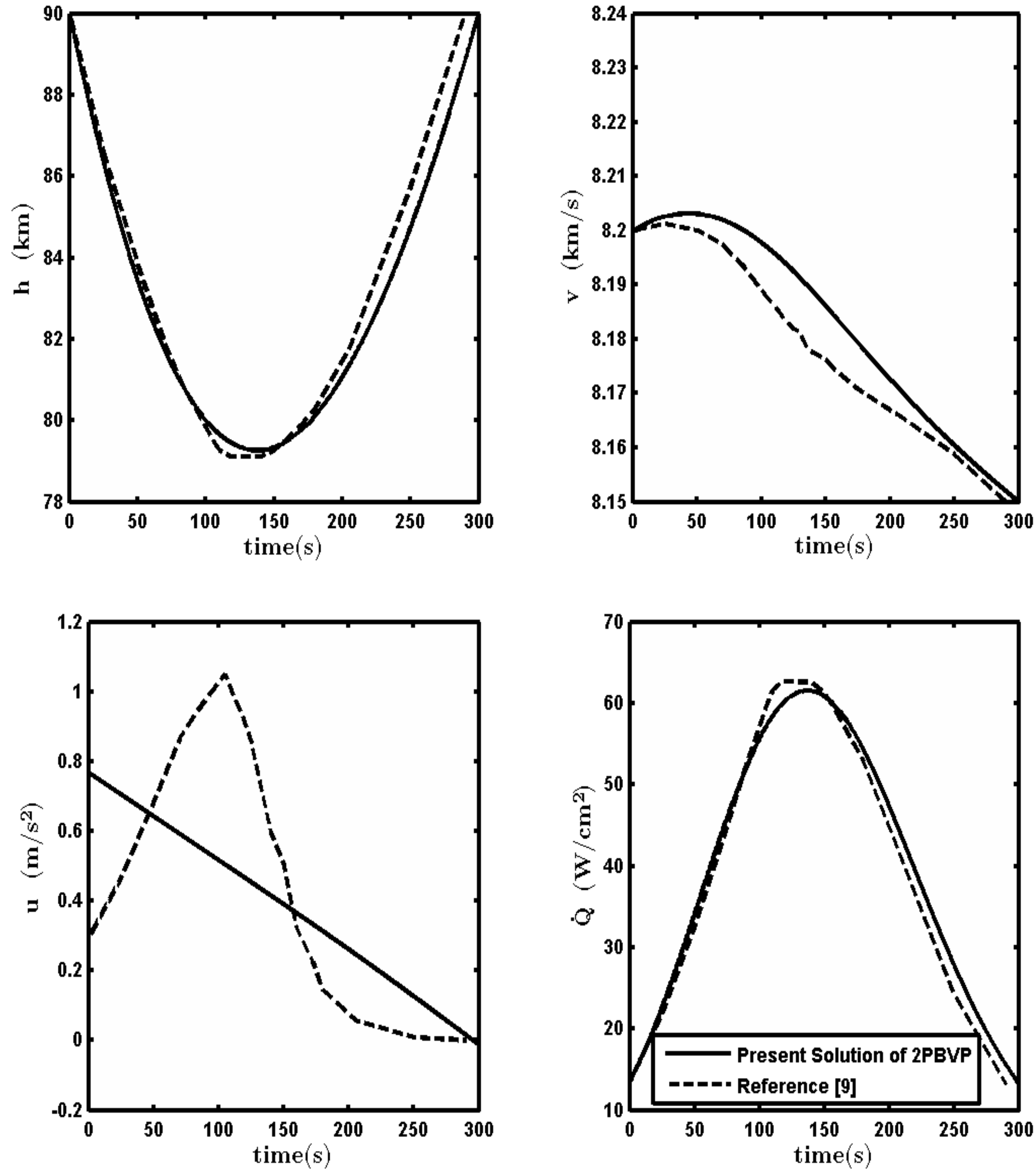

Figure 4.1: Comparison of the present solution of 2PBVP with the scheme presented in [9]

Table 4.1: Physical and mission constants

Constant	Value
r_0	6468.1 km
r_f	6468.1 km
v_0	8.2 km/s
v_f	8.15 km/s
γ_0	-0.02 rad
γ_f	0.0144 rad
t_0	0 s
t_f	300 s
R	1
ρ_s	1.752 kg/m^3
H	7.045 km
R_e	6378.1 km
g	9.81 m/s^2
C_{D_0}	0.1
m/S	300 kg/m^2

time which was left free in the case of the former, while it is fixed in the case of latter. A major difference can also be observed with regard to the objective function, the present case aims at minimizing the control effort while [9] intends to maximize the negative non-dimensional exit velocity given by:

$$J = -v_f^* = -ln\left(\frac{v_f}{\sqrt{\mu R_e}}\right) \tag{4.1}$$

Fig.4.1 presents the comparison for the altitude, velocity, normal acceleration (control variable in the present case) and heating rate of the spacecraft. The following are the relative merits of the present scheme as opposed to the one used in [9]:

1. The minimum altitude of the trajectory in the present scheme is observed to be smaller. It is important to note that the exit velocities for both schemes are same. The spacecraft in the present scheme could achieve the same amount of deceleration by descending to a smaller altitude.

2. The magnitude of maximum control effort (normal acceleration) is also observed to be considerably smaller.

3. The total control power required in the present scheme is observed to be smaller by 22.324 m/s than that used in [9]. The total control power is the integral of the control variable over t, from t_0 to t_f.

4. The maximum heating rate is smaller by 2.5 W/cm^2 in the present scheme.

5. The variation of the control variable u (normal acceleration) over t is observed to be linear for the given boundary conditions.

4.2 Time-Linearity of Optimal Control Law

From Figure 4.1 we can observe that the control variable u appears to vary linearly with time. By considering the optimum control law given by (3.20) and differentiating it with respect to time, an analytical expression for du/dt is obtained given by (4.2).

$$\begin{aligned} \frac{du}{dt} &= \left(\frac{-1}{2R}\right)\left(-\lambda_r \cos\gamma + \frac{\lambda_v g \cos\gamma}{v} + \frac{\lambda_\gamma \sin\gamma}{r} + K\lambda_\gamma \mathrm{e}^{-(r-R_e)/H}\right) \\ \frac{du}{dt} &= \left(\frac{-1}{2R}\right)(c_1 + c_2 + c_3 + c_4) = \left(\frac{-1}{2R}\right) c \end{aligned} \tag{4.2}$$

where,

$$c_1 = -\lambda_r \cos\gamma \tag{4.3}$$

$$c_2 = \frac{\lambda_v g \cos\gamma}{v} \tag{4.4}$$

$$c_3 = \frac{\lambda_\gamma \sin\gamma}{r} \tag{4.5}$$

$$c_4 = K\lambda_\gamma \mathrm{e}^{-(r-R_e)/H} \tag{4.6}$$

$$c = c_1 + c_2 + c_3 + c_4 \tag{4.7}$$

The variation of the four constituent terms in this equation ($-\lambda_r \cos\gamma$, $\frac{\lambda_v g \cos\gamma}{v}$, $\frac{\lambda_\gamma \sin\gamma}{r}$ and $K\lambda_\gamma \mathrm{e}^{-(r-R_e)/H}$) with respect to time is plotted in Figure 4.2 and compared with their sum (c). It can be observed that the contribution of c_3 and c_4 towards c is negligible. So, the sum of c_1 and c_2 gives c, which varies only in the order of mm/sec^3 and hence can be approximated to a constant.

4.3 Approximate Closed-form Solution with time-linear control

For the boundary conditions used in the nominal case discussed in the previous section, the optimal control law can be approximated to a straight line with respect to its variation in time, as described in Fig. 4.2. Closed-form solutions for (2.7) are not common but with the assumption that the control law is linear in time, it is possible to obtain an approximate one. Occasionally, it is also required to estimate the state

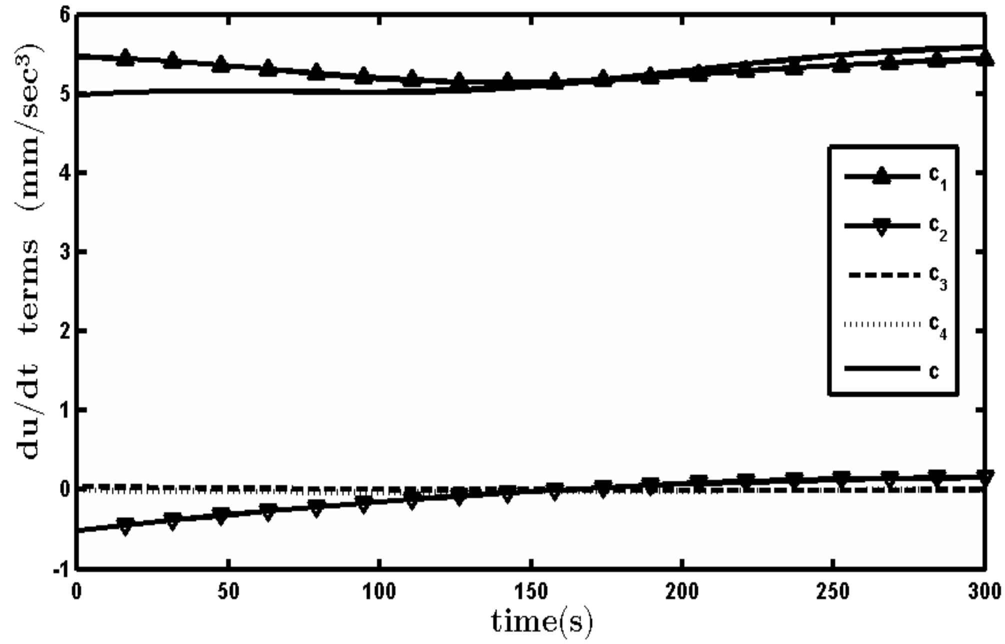

Figure 4.2: Comparison between the various terms contributing to the control time derivative

of the AOT vehicle at a given instant of time. Solving the non-linear state equations might prove to be computationally very expensive. Hence, there is a need to derive approximate closed-form solutions for the state equations, so that the states can be computed directly. An approximate closed-form solution for a time-linear control law is derived and presented in this section. The time-linear control law is given by the following expression.

$$u = a + bt \tag{4.8}$$

The following assumptions were made, to obtain the approximate solution:

1. At any instant of time during the atmospheric pass, the flight path angle is assumed to be small.

$$\sin\gamma \approx \gamma \qquad and \qquad \cos\gamma \approx 1 \tag{4.9}$$

2. v^2/rg called the Loh's term[8] is assumed to be constant in the equation for the flight path angle.

3. Speed of the AOT vehicle, v in equations for the radius and flight path angle are assumed to be constant.

4. The term $K\mathrm{e}^{-\frac{r-R_e}{H}}v$ is assumed to be constant and equal to $K\mathrm{e}^{-\frac{r_{avg}-R_e}{H}}v$ where r_{avg} is the average radial distance from the center of the earth.

The above assumptions applied on (2.7), lead to the following set of simpler equations.

$$\frac{\mathrm{d}r}{\mathrm{dt}} = v_0\gamma; \tag{4.10a}$$

$$\frac{\mathrm{d}v}{\mathrm{dt}} = -g\gamma - pv_0v; \qquad p = K\mathrm{e}^{-\frac{r_{avg}-R_e}{H}} \tag{4.10b}$$

$$\frac{\mathrm{d}\gamma}{\mathrm{dt}} = \frac{g(c-1)+a+bt}{v_0}; \qquad c = v_0^2/r_0g \tag{4.10c}$$

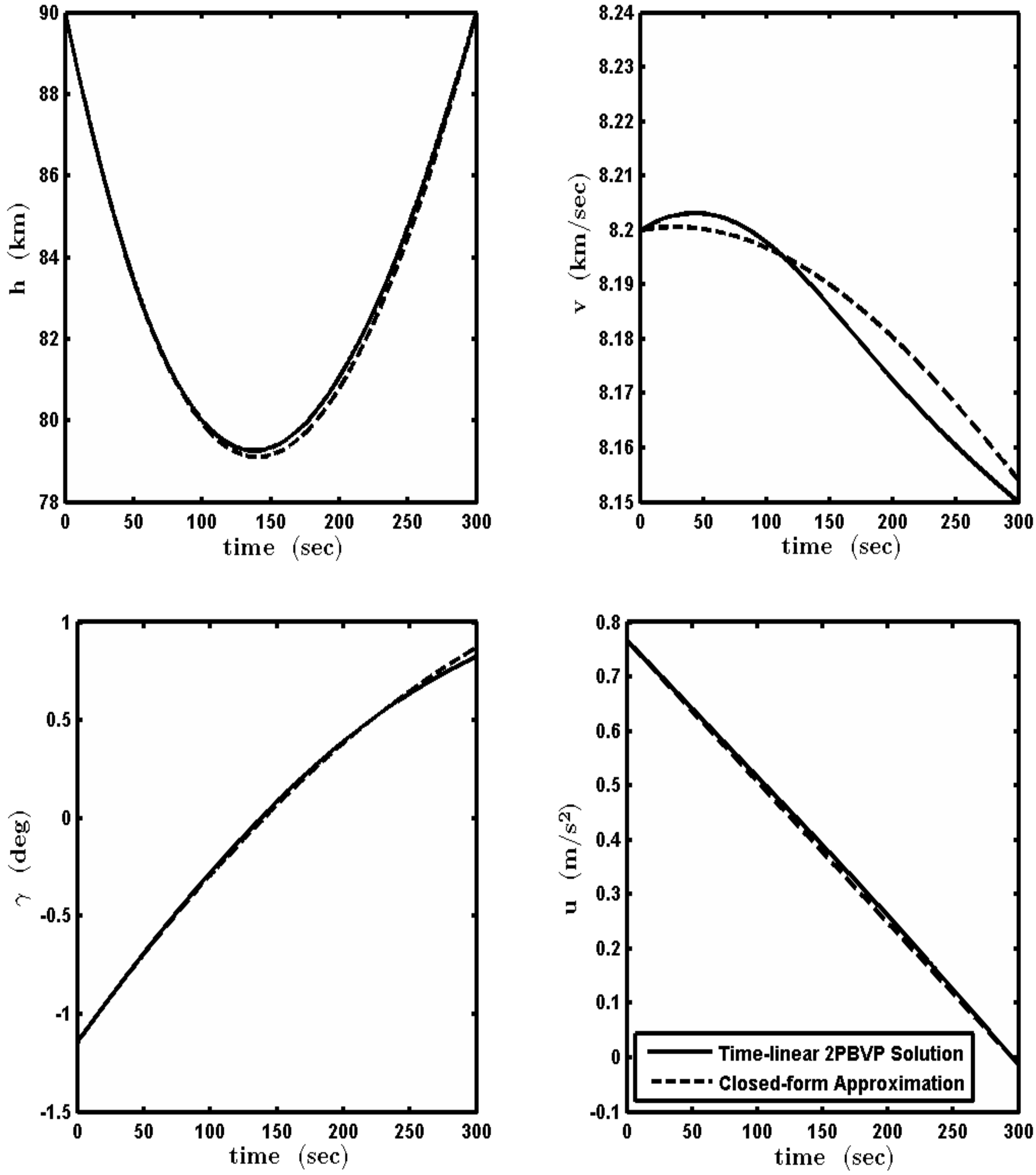

Figure 4.3: Comparison between the solution of 2PBVP and the approximate closed-form solution

Equation (4.10c) can be solved analytically and an expression for γ with respect to time can be obtained as follows,

$$\int_{\gamma_0}^{\gamma(t)} d\gamma = \int_0^t \left(\frac{g(c-1)+a}{v_0}\right) d\tau + \int_0^t \left(\frac{b}{v_0}\right) \tau d\tau \tag{4.11}$$

$$\gamma(t) = \gamma_0 + \left(\frac{g(c-1)+a}{v_0}\right) t + \left(\frac{b}{2v_0}\right) t^2 \tag{4.12}$$

This expression can be substituted into (4.10a) and we have,

$$\int_{r_0}^{r(t)} dr = \int_0^t \left(v_0\gamma_0 + (g(c-1)+a)\,\tau + \left(\frac{b}{2}\right)\tau^2\right) d\tau \tag{4.13}$$

$$r(t) = r_0 + (v_0\gamma_0)t + \left(\frac{g(c-1)+a}{2}\right) t^2 + \left(\frac{b}{6}\right) t^3 \tag{4.14}$$

Similarly (4.12) can be substituted into (4.10b), to get

$$\frac{dv}{dt} + pv_0 v = -g\gamma(t) \tag{4.15}$$

Multiplying both sides with e^{pv_0t},

$$\mathrm{e}^{pv_0t}\frac{dv}{dt} + pv_0 v\mathrm{e}^{pv_0t} = -g\mathrm{e}^{pv_0t}\gamma(t) \tag{4.16}$$

$$\frac{d\left(v\mathrm{e}^{pv_0t}\right)}{dt} = -g\mathrm{e}^{pv_0t}\gamma(t) \tag{4.17}$$

$$v\mathrm{e}^{pv_0t} = v_0 - g\int_0^t \mathrm{e}^{pv_0\tau}\gamma(\tau)d\tau \tag{4.18}$$

By solving the above equation, we have

$$\begin{aligned} v(t) = v_0 \mathrm{e}^{-pv_0 t} + \left(\frac{g}{pv_0}\right)\left(-\gamma_0 + \frac{g(c-1)+a}{pv_0{}^2} - \frac{b}{p^2 v_0{}^3}\right)(1-\mathrm{e}^{-pv_0 t}) \\ - \left(\frac{g}{pv_0}\right)\left(\frac{g(c-1)+a}{v_0} - \frac{b}{pv_0{}^2}\right) t - \left(\frac{g}{pv_0}\right)\left(\frac{b}{2v_0}\right) t^2 \end{aligned} \tag{4.19}$$

The approximate closed-form analytical solutions are given by (4.20), (4.21) and (4.22).

$$r = r_0 + (v_0\gamma_0)t + \left(\frac{g(c-1)+a}{2}\right)t^2 + \left(\frac{b}{6}\right)t^3 \tag{4.20}$$

$$\begin{aligned} v = & v_0 \mathrm{e}^{-pv_0 t} + \left(\frac{g}{pv_0}\right)\left(-\gamma_0 + \frac{g(c-1)+a}{pv_0{}^2} - \frac{b}{p^2 v_0{}^3}\right)(1-\mathrm{e}^{-pv_0 t}) \\ & - \left(\frac{g}{pv_0}\right)\left(\frac{g(c-1)+a}{v_0} - \frac{b}{pv_0{}^2}\right) t - \left(\frac{g}{pv_0}\right)\left(\frac{b}{2v_0}\right) t^2 \end{aligned} \tag{4.21}$$

$$\gamma = \gamma_0 + \left(\frac{g(c-1)+a}{v_0}\right)t + \left(\frac{b}{2v_0}\right)t^2 \tag{4.22}$$

$$\begin{aligned} \textit{where} \quad r_{avg} = & r_0 + \frac{v_0\gamma_0}{2} t_f + \left(\frac{g(c-1)+a}{6}\right)t_f^2 + \left(\frac{b}{24}\right)t_f^3; \\ p = & K\mathrm{e}^{-\frac{r_{avg}-R_e}{H}}; \end{aligned}$$

A comparison between the approximate closed-form solution and the solution of two-point boundary value problem is presented in Fig. 4.3. It can be observed that the optimal trajectory is close to the trajectory obtained through the approximate closed-form solution. It is important to note that the closed-form solution assumes that the control law is linear, hence the validity of the closed-form solution depends on the linearity of the optimal control law.

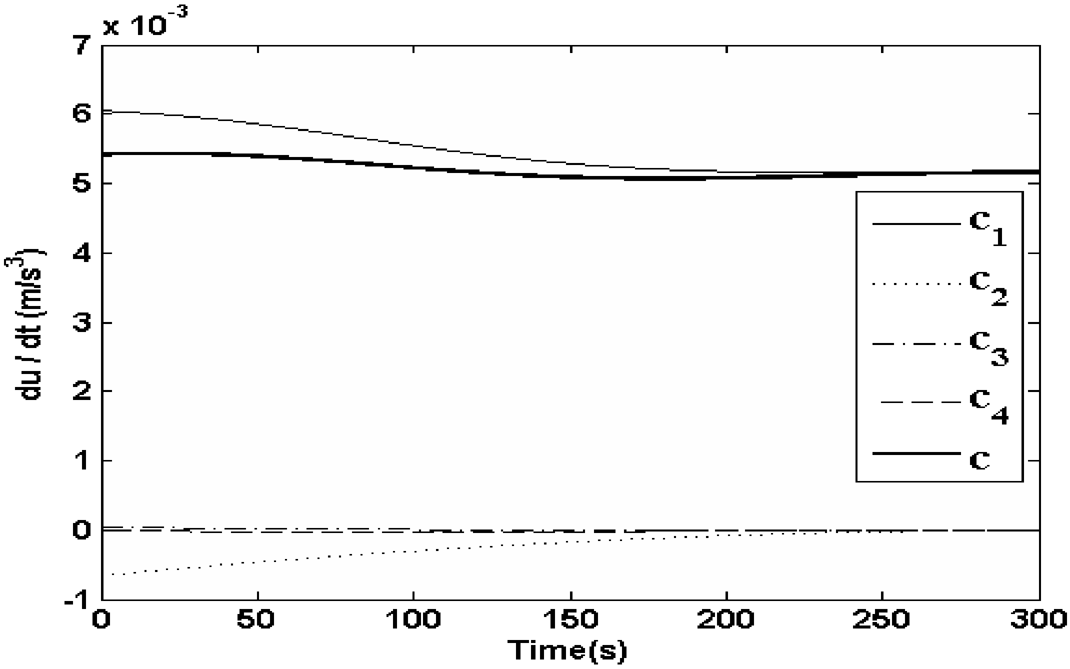

Figure 4.4: Comparison between the various terms contributing to the control time derivative

4.4 Time-Linear Empirical Relation for Free Exit Velocity

As an alternative to the time-linearity study of the 2PBVP discussed in section 4.2, a study was conducted to analyze the solution of section 4.1 if the exit velocity is considered as a free boundary condition. It was observed that if the exit velocity is left free, the time-linear solution is found to be typical and an analysis was done explaining the reasons for linearity of the control law, in this case.

It can be observed from Figure 4.4 that c_1 $(-\lambda_r \cos\gamma)$ has the maximum contribution towards du/dt as compared to the other terms. Though it might appear that c_1 is a close approximation to c, it is important to note that the value of c_1 at t_f is a better approximation than c_1 itself and also makes the approximate du/dt a constant, as $\gamma(t_f)$

is very small. From Figure 4.1, we can see that $u\Big|_{t_f}$ reaches zero which gives us the point $(t_f, 0)$. Hence, the Approximate Time Linear Optimal Control Law is given by Eq (4.23).

$$u(t)\Big|_{approx} = \left(\frac{-\lambda_r(t_f)}{2R}\right)(t_f - t) \tag{4.23}$$

Now let us investigate the assumption of constant slope from an analytical point of view.

The slope of the control variable u will remain constant if:

$$\frac{du}{dt}\Big|_{t_0} = \frac{du}{dt}\Big|_{t_0+h} = \ldots = \frac{du}{dt}\Big|_{t_0+(n-1)h} = \frac{du}{dt}\Big|_{t_f}$$

The greater the number of conditions, the smaller will be the range of values satisfying this condition. So, the least we can expect is for the slopes to be equal at t_0 and t_f, hoping it wouldn't change much in between. This would give us the following expression:

$$\lambda_r(t_0) - \frac{\lambda_v(t_0)g}{v_0} \approx \lambda_r(t_f) - \frac{\lambda_v(t_f)g}{v_f}$$

Typically we would want $v_0 - v_f$ to be as high as possible, this would enforce a very strict condition on $\lambda_r(t_0)$ and $\lambda_r(t_f)$. This will not be the case if $\lambda_v(t_f)$ is forced to be zero by making v_f a free boundary condition. The above strict condition can be split into two lenient conditions:

$$\lambda_v(t_f) = 0 \tag{4.24}$$

$$\lambda_r(t_0) - \frac{\lambda_v(t_0)g}{v_0} \approx \lambda_r(t_f) \tag{4.25}$$

Hence, K_1 was chosen to be zero. The following conditions influence (approximate) linearity of u or the extent of it:

1. For (approximate) linearity of u at least Eq (4.24) has to be satisfied but satisfying this condition does not ensure linearity.

2. If Eq (4.25) is satisfied then (approximate) linearity is ensured, the extent to which this condition is violated will decide the extent of non-linearity.

From the above conditions, it can be seen that the linearity depends on the boundary values of the Lagrange Multipliers. The boundary values of the Lagrange Multipliers are influenced by the boundary values of the state vector. Hence, it can be concluded that the linearity of u depends on the boundary conditions of the optimization problem. The boundary conditions in Table 4.1 sufficiently satisfy these conditions and hence are considered as reference boundary conditions. It was observed that u stays approximately linear if the given boundary conditions are in the same ratio as the reference boundary conditions, for reentry Altitude (h_0) ranging from 83 km - 115 km. The following steps have to be followed:

1. A reentry altitude (h_0) betwwen 83 km - 115 km has to be chosen.

2. Reentry flight path angle (γ_0) has to be obtained from Eq (4.26) for the chosen h_0.

$$\gamma_0 = h_0 \left(\frac{-0.02}{90} \right); \qquad \text{where } h_0 \text{ is in } km \text{ and } \gamma_0 \text{ is in } rad \tag{4.26}$$

3. Reentry Velocity (v_0) has to be obtained from Eq (4.27) for the chosen h_0.

$$v_0 = h_0 \left(\frac{8.2}{90} \right); \qquad \text{where } h_0 \text{ is in } km \text{ and } v_0 \text{ is in } km/s \tag{4.27}$$

The above boundary conditions, along with $t_f = 300$ s (valid for $t_f < 400$ s) can be used to obtain a fairly linear solution for the optimization problem.

In Eq.(4.23), the value of $\lambda_r(t_f)$ can be obtained only after solving the 2PBVP. In order to avoid solving the 2PBVP, an empirical relation is obtained for $\lambda_r(t_f)$ in terms of the boundary conditions $h_0(= r_0 - R_e = r_f - R_e)$, v_0, γ_0 and fixed final time t_f. A variational approach was adopted, where three of these four values are kept constant while the fourth one is varied and the variation in $\lambda_r(t_f)$ is observed. This process is repeated for the other three values and the results are presented in Figure 4.5.

Newton's interpolation method is used to obtain empirical relationships between $\lambda_r(t_f)$ and the three boundary conditions along with t_f considered separately. The variation of $\lambda_r(tf)$ with respect to v_0 and γ_0 is observed to be almost linear but thats

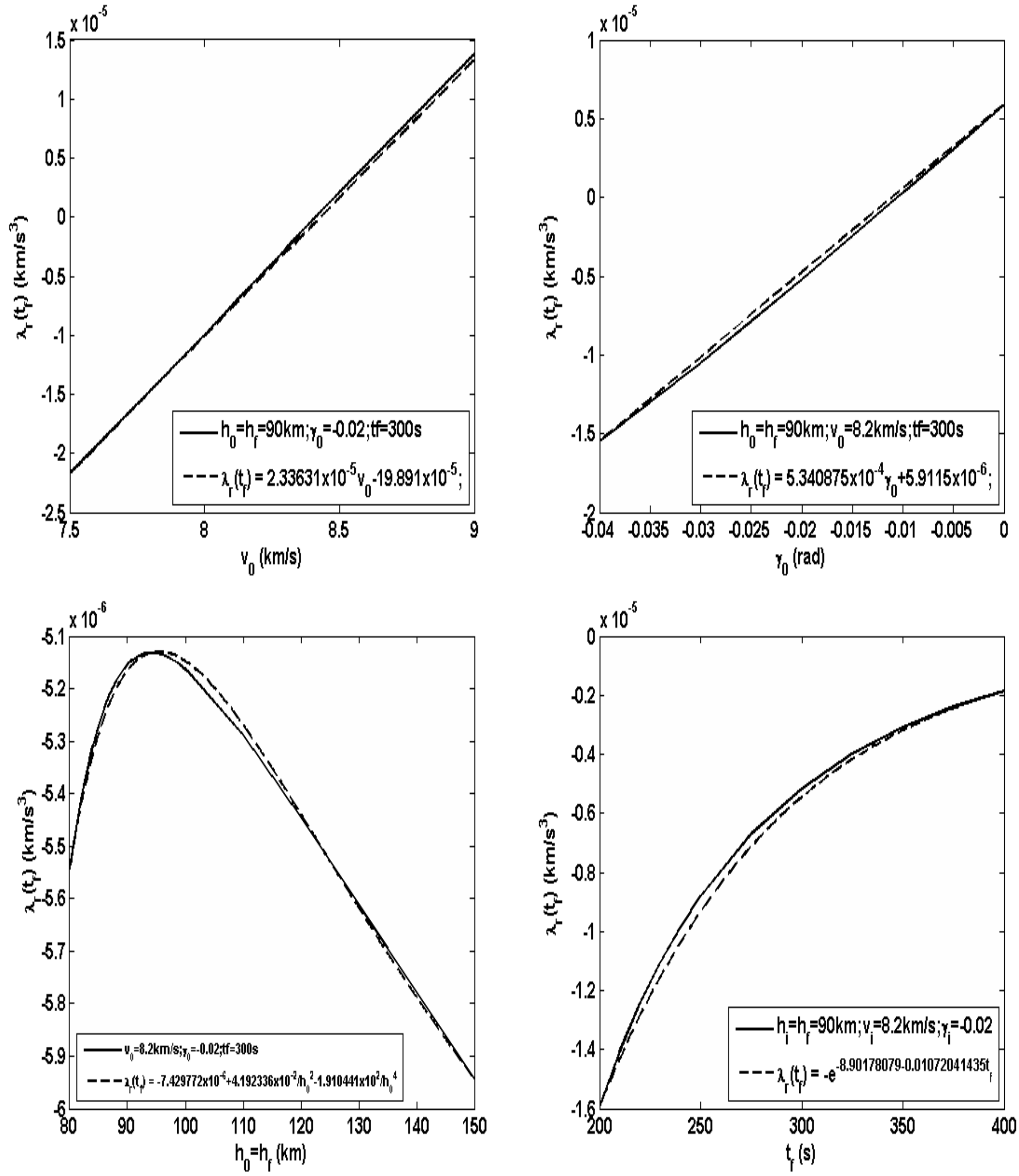

Figure 4.5: Variation of co-radial Lagrange parameter with entry conditions

not the case with h_0 and t_f. Considering the variation of $\lambda_r(t_f)$ with respect to h_0, it can be observed that $|\lambda_r(tf)|$ is at its minimum at an altitude of approximately $94km$ for the case when $v_0 = 8.2$ km/s, $\gamma_0 = -0.02$rad and $t_f = 300$ s. It is to be noted that the deceleration in terms of $v_0 - v_f$ decreases with increase in initial altitude h_0. So, it would be ideal to choose an initial altitude less than 94km, so as to get higher deceleration for the same control effort as shown in Figure 4.6.

Using the data in Figure 4.5, an empirical relation for $\lambda_r(t_f)$(in km/sec^3), given by Eq (4.28), is obtained in terms of v_0(in km/s), γ_0(in rad), h_0(in km) and t_f(in s).

$$\begin{aligned} \lambda_r(t_f)\Big|_{empirical} &= -1.828523 \times 10^{-4} + 2.3363 \times 10^{-5} v_0 + 5.340875 \times 10^{-4}\gamma_0 \\ &\quad +4.192336 \times 10^{-2}/h_0^2 - 1.910441 \times 10^{2}/h_0^4 \\ &\quad -1.3614626 \times 10^{-4} \mathrm{e}^{-0.01072041435 t_f} \end{aligned} \tag{4.28}$$

Fig.4.7-4.8 present the comparison between the 2PBVP solution the solution using the approximate time linear control law and the solution using the empirical relation obtained in Eq.(4.28).

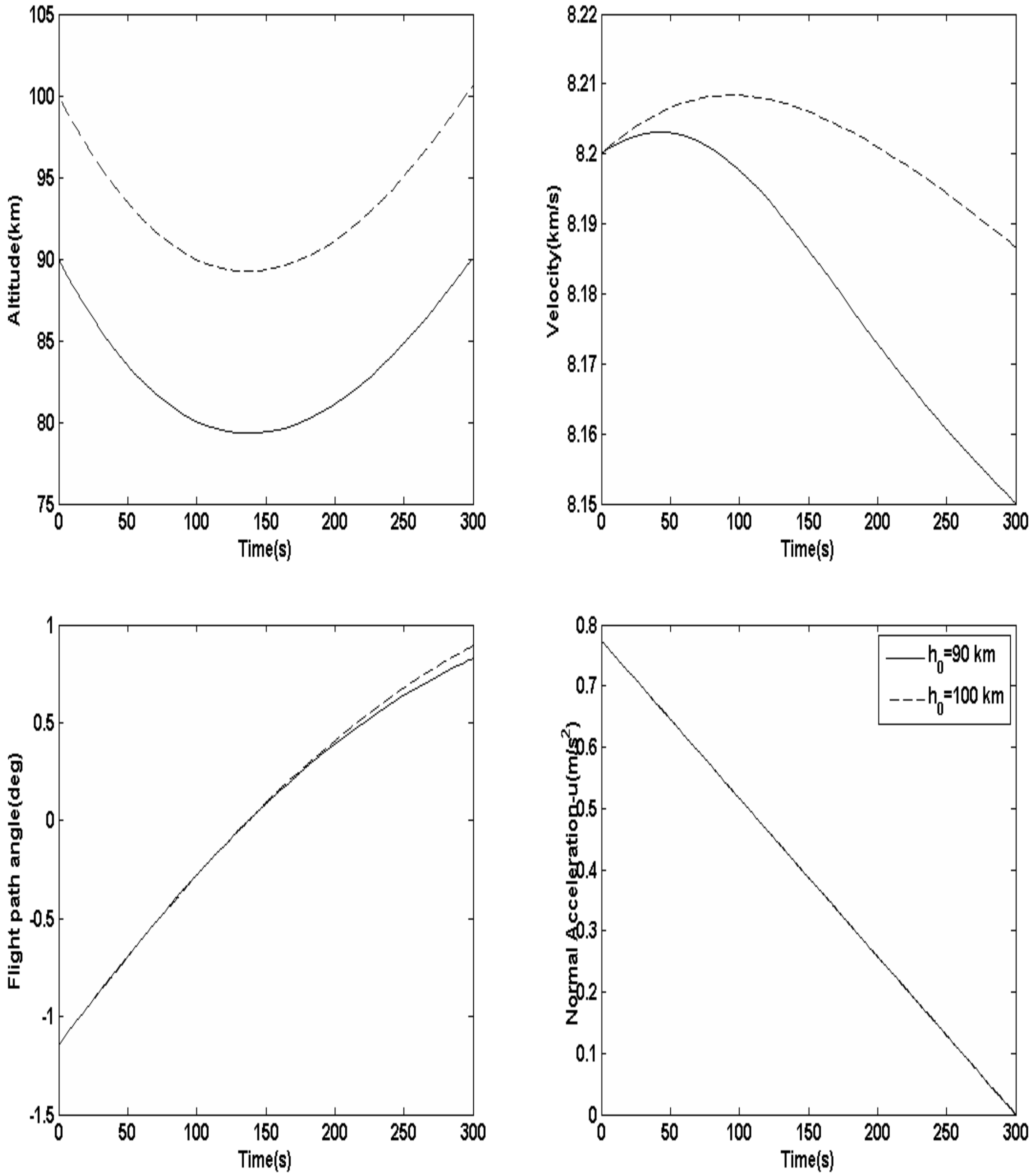

Figure 4.6: Comparison of results between h_0=90 km and h_0=100 km, with v_0=8.2 km/s, γ_0=-0.02 rad and t_f=300 s using an approximate time-linear optimal control law

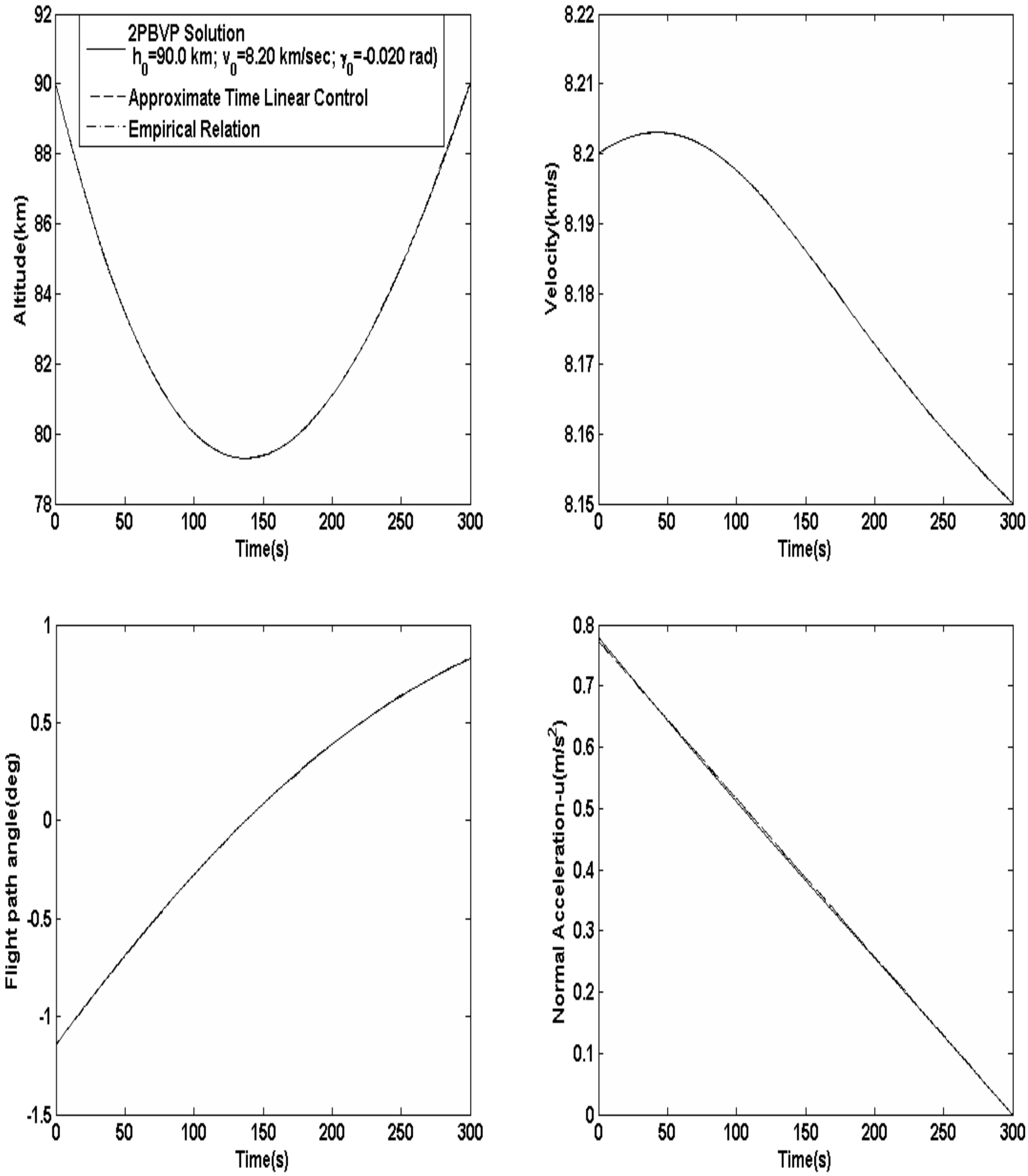

Figure 4.7: Comparison between the solution of 2PBVP, results with approximate control law and results obtained using empirical relation for reference boundary conditions

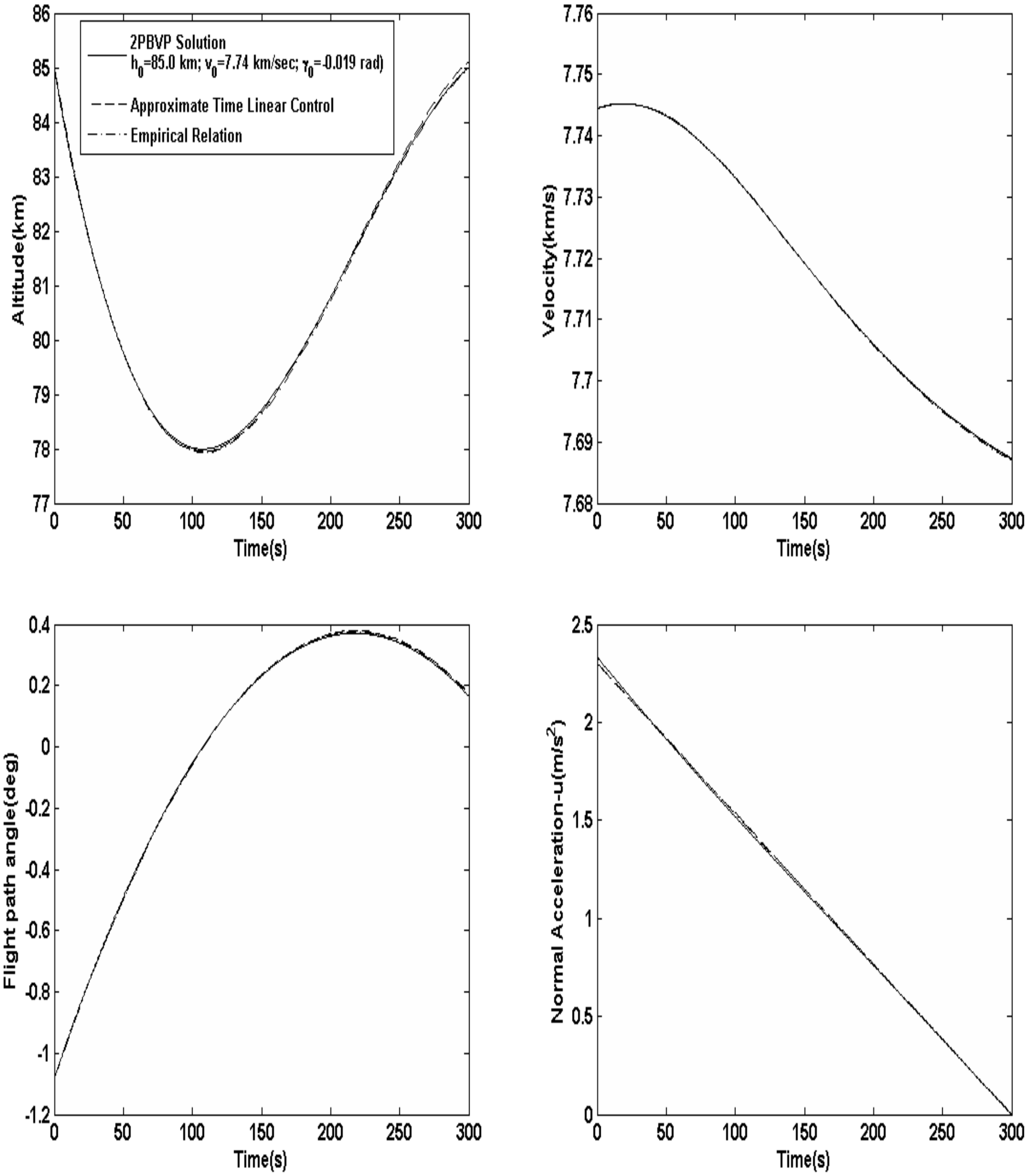

Figure 4.8: Comparison between the solution of 2PBVP, results with approximate control law and results obtained using empirical relation for boundary conditions proportional to the reference ones

5

Linear Quadratic Regulator

The AOT discussed here is from a HEO to a LEO involving a deorbit impulse at the HEO, a pass through the upper reaches of atmosphere and a reorbit impulse at the LEO. The reentry conditions for the atmospheric pass essentially depend on the deorbit impulse, if this impulse is not executed as planned it might lead to different reentry conditions. Hence, it would be helpful to have a feedback control system which can compensate the initial perturbations during reentry and ensure the AOT vehicle exits with desired conditions. Naidu et al. [12] emphasizes on the need to take the possibility of deviations in initial conditions into account. Such deviations might affect the outcome of a mission as they might lead to deviations in exit conditions which is not desirable. Hence, linear quadratic regulator is chosen to compensate the expected deviations in initial conditions for the linearized state equations given by (5.1).

$$\boldsymbol{\delta}\dot{\mathbf{x}} = A\boldsymbol{\delta}\mathbf{x} + B\delta u \tag{5.1}$$

where,

$$A = \begin{pmatrix} 0 & \sin\gamma_d & v_d\cos\gamma_d \\ (K/H)\mathrm{e}^{-(r_d-R_e)/H}v_d^2 & -2K\mathrm{e}^{-(r_d-R_e)/H}v_d & -g\cos\gamma_d \\ -v_d/{r_d}^2 & \left(\frac{1}{r_d}+\frac{g}{{v_d}^2}\right)\cos\gamma_d - \frac{u_d}{{v_d}^2} & -\left(\frac{v_d}{r_d}-\frac{g}{v_d}\right)\sin\gamma_d \end{pmatrix}; \tag{5.2}$$

$$B = \begin{Bmatrix} 0 \\ 0 \\ 1/v_d \end{Bmatrix} \tag{5.3}$$

and

$$\boldsymbol{\delta}\mathbf{x}(t_0) \tag{5.4}$$

is the initial perturbation to be compensated. The matrices A and B are frozen at $t = 0$, so that (5.1) becomes linear-time invariant system. It is also observed that (A, B) is controllable. The following LQRs were designed and the results are presented.

5.1 Infinite-Time LQR

In this section, an infinite-time tracking linear quadratic regulator is implemented as described in [17]. The regulator is designed for a set of linearized state equations given by (5.1) to minimize the following cost function:

$$J = \frac{1}{2}\int_{t_0}^{\infty} (\boldsymbol{\delta}\mathbf{x}^T Q \boldsymbol{\delta}\mathbf{x} + \delta u^T R \delta u) dt \tag{5.5}$$

$$where, \qquad R = 3.33 \times 10^7; \qquad Q = \begin{pmatrix} 0.33 & 0 & 0 \\ 0 & 3.3 \times 10^5 & 0 \\ 0 & 0 & 3.3 \times 10^5 \end{pmatrix} \tag{5.6}$$

Additionally, $(A, \sqrt{Q})$ is found to be observable. The control law for this regulator is given by,

$$\delta u = -\mathbf{k}^T \boldsymbol{\delta}\mathbf{x} \tag{5.7}$$

with

$$\mathbf{k}^T = R^{-1} B^T M_0 \tag{5.8}$$

where M_0 is the solution of the following algebraic Riccati equation

$$A^T M_0 + M_0 A - M_0 B R^{-1} B M_0 + Q = \emptyset \tag{5.9}$$

This LQR is implemented and the results are presented in Fig. 5.1. It can be observed that the regulator fails to reach the exit conditions for altitude and flight path angle, which is undesirable. Various sets of Q and R were tried by trail and error and the respective % error in Altitude, velocity and flight path angle are presented in Table 5.1. It can be observed from the table that among a wide range of Q and R values the ones used in implementing the LQR in this section prove to have the best performance and yet it is not sufficient to satisfy the exit conditions.

Table 5.1: Performance analysis of infinite time LQR

Q(1,1)	Q(2,2)	Q(3,3)	R	% Error in h	% Error in v	% Error in γ
3.3×10^{-1}	3.3×10^{5}	3.3×10^{5}	3.3×10^{1}	-8.330947×10^{-1}	-7.674506×10^{-3}	1.328529×10^{-4}
3.3×10^{-1}	3.3×10^{5}	3.3×10^{5}	3.3×10^{3}	-8.312663×10^{-1}	-7.626646×10^{-3}	1.302752×10^{-4}
3.3×10^{-1}	3.3×10^{5}	3.3×10^{5}	3.3×10^{5}	-8.136856×10^{-1}	-7.266482×10^{-3}	1.625764×10^{-4}
3.3×10^{-1}	3.3×10^{5}	3.3×10^{5}	3.3×10^{6}	-8.149946×10^{-1}	-6.148191×10^{-3}	3.622559×10^{-4}
3.3×10^{-3}	3.3×10^{5}	3.3×10^{5}	3.3×10^{6}	-6.685509×10^{-1}	-7.426417×10^{-3}	4.637773×10^{-4}
3.3×10^{-5}	3.3×10^{5}	3.3×10^{5}	3.3×10^{6}	-6.676998×10^{-1}	-7.439671×10^{-3}	4.646589×10^{-4}
3.3×10^{-5}	3.3×10^{3}	3.3×10^{5}	3.3×10^{6}	-1.870836	2.218201×10^{-2}	-9.037782×10^{-4}
3.3×10^{-5}	3.3×10^{6}	3.3×10^{5}	3.3×10^{6}	-9.089321×10^{-1}	-1.792623×10^{-2}	-1.288355×10^{-3}
3.3×10^{-5}	3.3×10^{7}	3.3×10^{5}	3.3×10^{6}	-2.184688	-2.715541×10^{-2}	-1.952334×10^{-3}
3.3×10^{-3}	3.3×10^{5}	3.3×10^{5}	3.3×10^{7}	-1.752500	-7.499659×10^{-4}	1.269265×10^{-3}
3.3×10^{-5}	3.3×10^{5}	3.3×10^{5}	3.3×10^{7}	-1.753156	-7.559092×10^{-4}	1.269595×10^{-3}
3.3×10^{-5}	3.3×10^{6}	3.3×10^{5}	3.3×10^{7}	1.248446×10^{-1}	-1.353054×10^{-2}	-4.437157×10^{-4}
3.3×10^{-5}	3.3×10^{6}	3.3×10^{5}	3.3×10^{7}	1.248446×10^{-1}	-1.353054×10^{-2}	-4.437157×10^{-4}
3.3×10^{-5}	1.6×10^{6}	3.3×10^{5}	3.3×10^{7}	-4.032234×10^{-2}	-1.063721×10^{-2}	5.250472×10^{-4}
3.3×10^{-1}	1.6×10^{4}	3.3×10^{5}	3.3×10^{7}	-2.332694	2.013555×10^{-2}	-4.883690×10^{-4}
3.3×10^{-1}	1.6×10^{5}	3.3×10^{5}	3.3×10^{7}	-2.346540	5.351797×10^{-3}	8.535150×10^{-4}
3.3×10^{-1}	1.6×10^{6}	3.3×10^{3}	3.3×10^{7}	1.747784×10^{-1}	-1.179445×10^{-2}	3.113647×10^{-4}
3.3×10^{-1}	1.6×10^{6}	3.3×10^{4}	3.3×10^{7}	1.716576×10^{-1}	-1.160233×10^{-2}	3.448520×10^{-4}
3.3×10^{-1}	1.6×10^{6}	3.3×10^{5}	3.3×10^{7}	-9.101259×10^{-2}	-1.024035×10^{-2}	4.822324×10^{-4}
3.3×10^{-1}	1.6×10^{6}	3.3×10^{6}	3.3×10^{7}	-1.327279	-2.745046×10^{-3}	6.353175×10^{-4}
3.3×10^{-1}	1.6×10^{6}	6.6×10^{6}	3.3×10^{7}	-1.852259	1.168006×10^{-3}	4.461293×10^{-4}
3.3×10^{-1}	1.6×10^{6}	3.3×10^{7}	3.3×10^{7}	-2.424546	1.145404×10^{-2}	-3.463410×10^{-4}
3.3×10^{-1}	1.6×10^{6}	1.6×10^{6}	3.3×10^{7}	-8.314880×10^{-1}	-6.198634×10^{-3}	6.769417×10^{-4}
3.3×10^{-1}	1.6×10^{6}	1.6×10^{6}	3.3×10^{8}	-2.373855	3.485764×10^{-3}	1.123891×10^{-3}
3.3×10^{-1}	1.6×10^{6}	1.6×10^{6}	3.3×10^{6}	-7.140788×10^{-1}	-8.136526×10^{-3}	2.283034×10^{-4}
3.3×10^{-1}	1.6×10^{6}	1.6×10^{6}	3.3×10^{5}	-7.320844×10^{-1}	-8.557474×10^{-3}	1.704078×10^{-4}
3.3×10^{-1}	1.6×10^{6}	1.6×10^{6}	3.3×10^{3}	-7.401844×10^{-1}	-8.757698×10^{-3}	1.619790×10^{-4}
3.3×10^{-1}	1.6×10^{6}	1.6×10^{6}	3.3×10^{1}	-7.392028×10^{-1}	-8.756616×10^{-3}	1.621789×10^{-4}
3.3×10^{-1}	3.3×10^{5}	3.3×10^{5}	3.3×10^{7}	-1.684028	-1.429151×10^{-5}	1.239149×10^{-3}

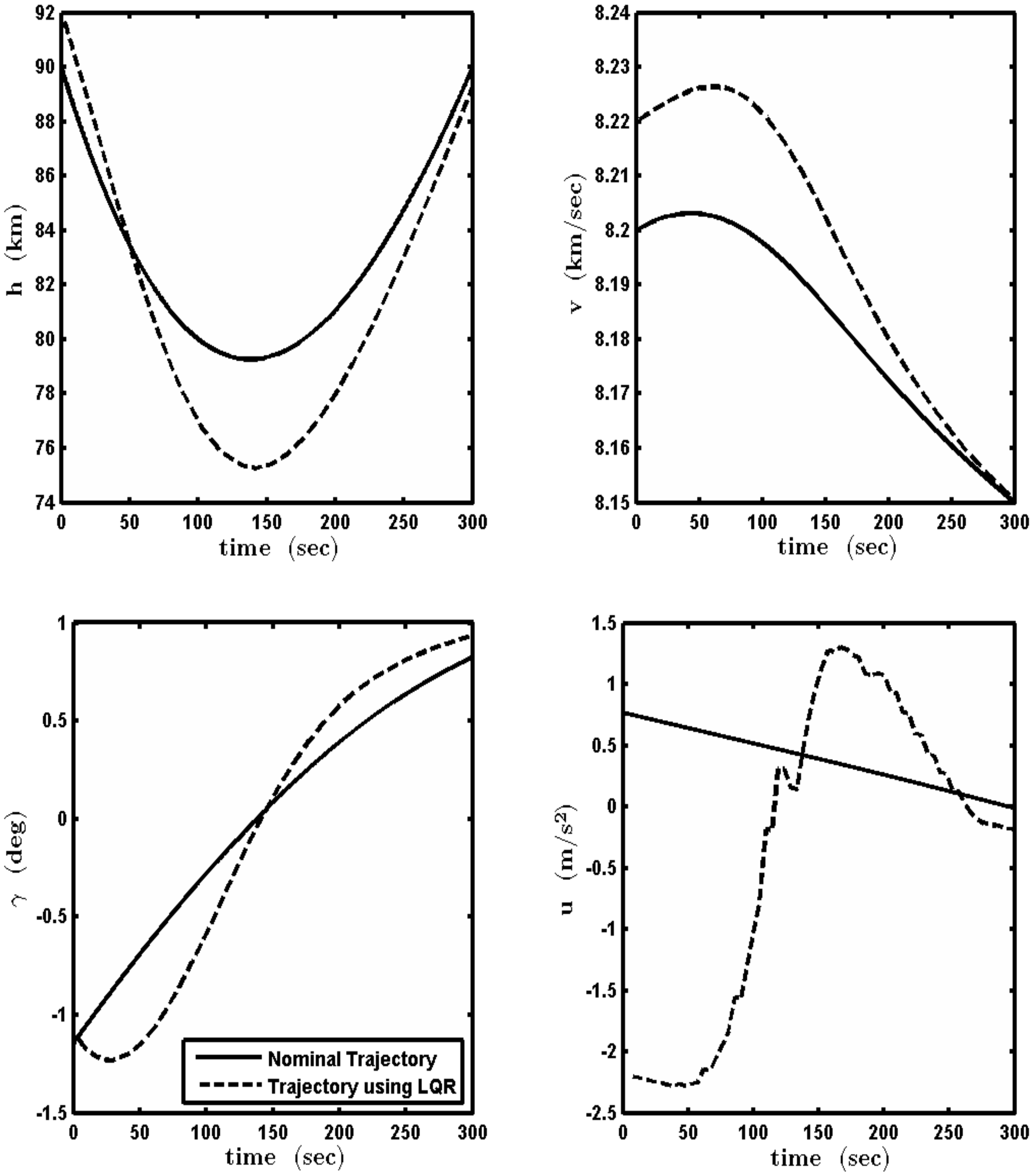

Figure 5.1: Comparison between the desired trajectory and the trajectory with perturbed initial state using an infinite time LQR

5.2 Terminal-Time LQR

In this section, a terminal-time tracking linear quadratic regulator is implemented as described in [17]. The regulator is designed for a set of linearized state equations to minimize the following cost function:

$$J = \frac{1}{2}\boldsymbol{\delta}\mathbf{x_f}^T V \boldsymbol{\delta}\mathbf{x_f} + \frac{1}{2}\int_{t_0}^{t_f} (\boldsymbol{\delta}\mathbf{x}^T Q \boldsymbol{\delta}\mathbf{x} + \delta u^T R \delta u) dt \tag{5.10}$$

$$where, \qquad R = 1; \qquad Q = \begin{pmatrix} 0 & 0 & 0 \\ 0 & 0 & 0 \\ 0 & 0 & 0 \end{pmatrix}; \qquad V = \begin{pmatrix} 1 & 0 & 0 \\ 0 & 0.5 & 0 \\ 0 & 0 & 0.05 \end{pmatrix}; \tag{5.11}$$

The control law for the terminal time LQR is given by,

$$\delta u = -\mathbf{k}^T \boldsymbol{\delta}\mathbf{x} \tag{5.12}$$

with

$$\mathbf{k}^T = R^{-1} B^T M_0 \tag{5.13}$$

where M_0 is the solution of the following Riccati equation

$$A^T M_0 + M_0 A - M_0 B R^{-1} B M_0 + Q = -\frac{\partial M_0}{\partial t} \tag{5.14}$$

subject to the terminal condition,

$$M_0(t_f) = V \tag{5.15}$$

The solution to the matrix Ricatti equation is given by, (see [17])

$$M_0 = EF^{-1} \tag{5.16}$$

with,

$$\begin{Bmatrix} F \\ E \end{Bmatrix} = \mathrm{e}^{\mathbf{H}(t-t_f)} \begin{Bmatrix} F(t_f) \\ E(t_f) \end{Bmatrix} \tag{5.17}$$

where,

$$\mathbf{H} = \begin{pmatrix} A & -BR^{-1}B^T \\ -Q & -A^T \end{pmatrix} \tag{5.18}$$

The initial state of the trajectory is perturbed from the desired trajectory and the above terminal time tracker is implemented to track the desired trajectory. The weighting matrices given above indicate that the emphasis is on minimizing the deviations in the states at terminal time. The linearized state equations for the system are given by (5.1). The terminal time LQR is applied to these state equations. A comparison between the desired trajectory and the trajectory with perturbed initial state using

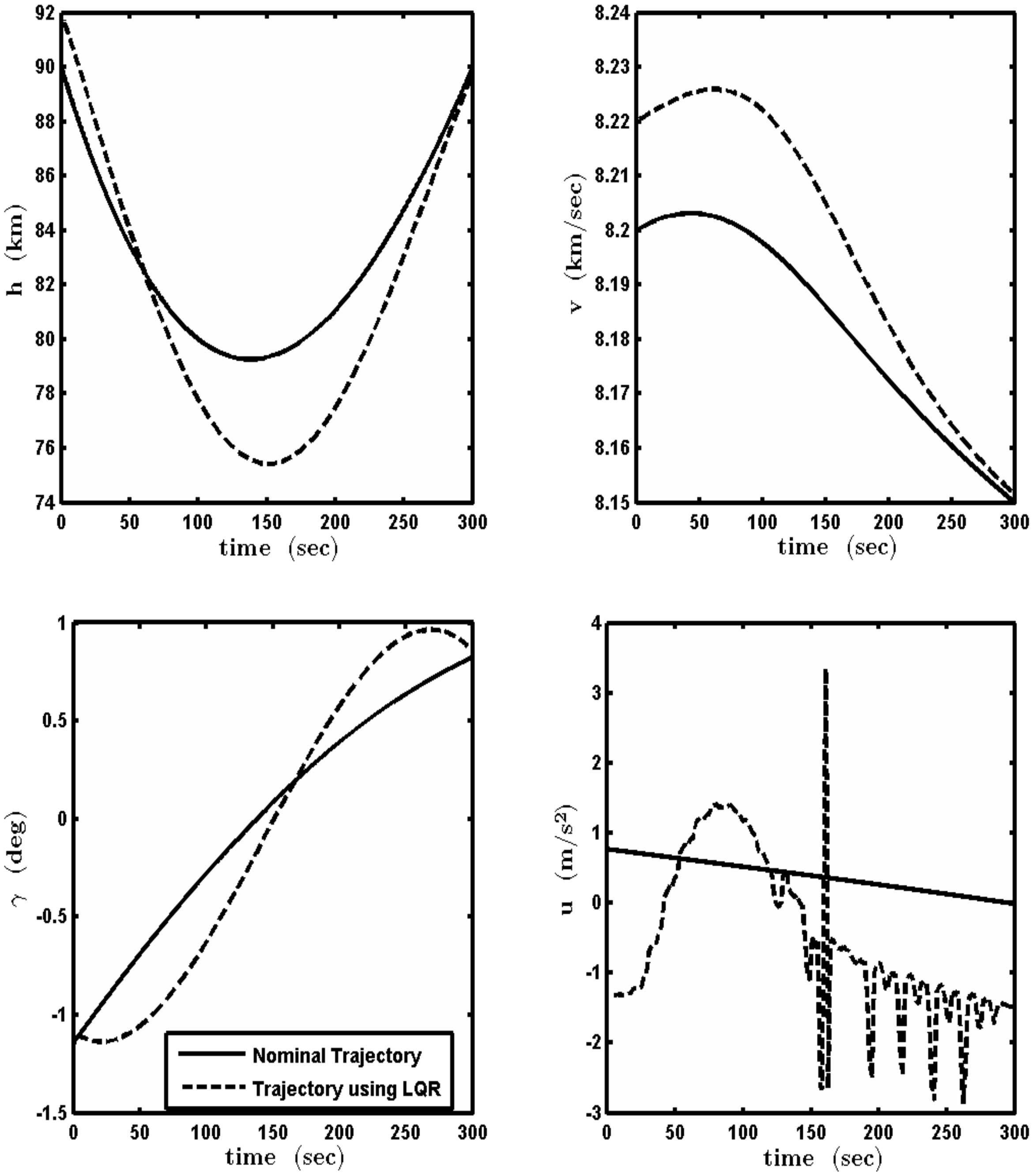

Figure 5.2: Comparison between the desired trajectory and the trajectory with perturbed initial state using a terminal time LQR

terminal time LQR is presented in Fig. 5.2. It can be clearly observed that there is a significant increase in control effort, magnitude of maximum control input and maximum heating rate (as the minimum altitude is smaller). Table 5.2 presents the performance analysis for the terminal time LQR where various combinations of Q, R and V were attempted and it can be seen that the best case was chosen.

Table 5.2: Performance analysis of terminal time LQR

Q(1,1)	Q(2,2)	Q(3,3)	R	V(1,1)	V(2,2)	V(3,3)	% δh	% δv	% $\delta\gamma$	$\lvert u\rvert_{max}$
0	0	0	1	1	0.5	0.1	5.66×10^{-3}	2.51×10^{-2}	4.85	3.013
0	0	0.02	1	1	0.5	0.1	7.86×10^{-3}	1.58×10^{-1}	2.62	3.015
0	0.02	0	1	1	0.5	0.1	8.32×10^{-3}	2.27×10^{-1}	-0.99	3.026
0	0.02	0.02	1	1	0.5	0.1	1.13×10^{-2}	2.71×10^{-1}	-1.51	3.012
0.0002	0	0	1	1	0.5	0.1	6.57×10^{-3}	2.75×10^{-1}	-0.89	3.685
0.0002	0.02	0.02	1	1	0.5	0.1	7.34×10^{-3}	2.76×10^{-1}	-0.98	3.694
0	0	0	1	1	0.5	0.2	7.27×10^{-3}	2.84×10^{-3}	8.91	3.028
0	0	0	1	1	0.5	0.05	6.83×10^{-3}	3.73×10^{-2}	2.62	3.015

6

Predictive Time-Linear Control

The terminal-time tracking system presented earlier suffers from two major drawbacks; the magnitude of the total control effort involved is larger and the maximum heating rate experienced by the AOT vehicle is higher, both of which are highly undesirable demanding a better control methodology to compensate for the deviations in reentry conditions. At this juncture we would like to draw some attention to the time linear property of the optimal control law. Having a linear control law in time can be very useful during the implementation phase as it can be easily implemented using a simple timing mechanism. Moreover, it is very easy to store this control law as we need to store only three parameters which are the control input at t=0, the slope of the control input with respect to time and the terminal time (referred as a, b and t_f respectively) instead of storing the entire control profile. Employing a tracking system is necessary for the following reasons:

1. If the vehicle re-enters the atmosphere with a higher speed than expected.

2. If the vehicle re-enters with a flight path angle different from the one used in the nominal case.

3. If the controller is deployed at a higher or a lower altitude as compared to the re-entry altitude.

In all the three scenarios mentioned above, there is a very good chance that the AOT vehicle might not exit the atmosphere with the desired conditions using the optimal control law obtained for the nominal case, which is crucial for the success of the mission. Hence, the control law will have to be adjusted in order to take the perturbed initial conditions into account. As the linearity of the control law obtained in the nominal case depends mainly on the boundary conditions, it is possible that the optimal control law obtained for the perturbed initial conditions might not result in a time-linear control profile. It is important to note that the optimal control law for the nominal case was obtained for a fixed final time condition and as far as the mission statement is concerned it is only important to exit the atmosphere with the desired exit conditions. So, the deviations in the initial conditions can be accounted for by spending a greater or a lesser amount of time inside the atmosphere depending on the initial conditions. But this still does not ensure that the control profile will be linear in time. So, we pose a new problem statement for the given mission. For the given perturbed initial conditions and desired exit conditions in order to obtain a time-linear control law what is the total time that is required to be spent within the atmosphere by the AOT vehicle and what are the values of a and b for this law?

As the above problem statement does not require the trajectory to be optimal, we can drop the costate equations in (3.21) and use only the state equations (2.7) with the control law given by (4.8) along with six boundary conditions completely describing the states of the vehicle at initial (perturbed initial conditions) and final time (which is free). Instead of solving a 2PBVP for a system of three first order ODEs with three unknown parameters (a, b and t'_f) and six boundary conditions, we consider solving a 2PBVP for a system of five first order ODEs and five boundary conditions as shown in (6.1) and (6.2) with fixed terminal time t'_f in order to ensure greater success in obtaining the solution.

$$\left\{\begin{array}{c}\dot{r}\\ \dot{v}\\ \dot{\gamma}\\ \dot{a}\\ \dot{b}\end{array}\right\} = \left\{\begin{array}{c} v\ \sin\gamma \\ -g\ \sin\gamma - K\mathrm{e}^{-\left(\frac{r-R_e}{H}\right)}v^2 \\ (v/r - g/v)\ \cos\gamma + (a+bt)/v \\ 0 \\ 0 \end{array}\right\} \tag{6.1}$$

$$\left\{\begin{array}{c} r(t_0)\\ v(t_0)\\ \gamma(t_0)\end{array}\right\} = \left\{\begin{array}{c} r'_0\\ v'_0\\ \gamma'_0\end{array}\right\}; \qquad \left\{\begin{array}{c} r(t_f)\\ v(t_f)\end{array}\right\} = \left\{\begin{array}{c} r_f\\ v_f\end{array}\right\}; \tag{6.2}$$

Then a Newton-Raphson technique (6.3) is used to iteratively find t'_f so that the exit flight path angle equals the desired flight path angle, as in the case of shooting method, using the closed form approximation (4.22) to obtain the partial derivative of the exit flight path angle ($\gamma(t'_f)$) with respect to the final time (t'_f).

$$t'_f = t'_f + \frac{\gamma(t'_f) - \gamma_f}{\frac{\partial \gamma(t'_f)}{\partial t'_f}} \tag{6.3}$$

$$where, \qquad \frac{\partial \gamma(t'_f)}{\partial t'_f} = \left(\frac{g(c-1)+a}{v_0}\right) + \left(\frac{b}{v_0}\right) t'_f \tag{6.4}$$

The block diagram for the predictive time-linear control algorithm described here is presented in Fig. 6.1. Through this exercise, we can obtain t'_f which is the new final time for the perturbed initial conditions. The values of parameters a and b obtained from the final 2PBVP solved will define the time-linear control profile required for the maneuver which satisfies all the given six boundary conditions.

The only question to be answered now, is this time-linear control law an optimal one or not? If not then how close or how far is it from the optimal solution? In order to answer these questions, a comparison between the trajectory obtained using predictive time-linear control and the optimal trajectory for the same six boundary conditions with t'_f as the final time is presented in Fig. 6.2. It can be observed that the optimal control input profile is close to the time-linear one. The former is observed to be oscillating about the latter thus making the cost function approximately the same for both the cases, which is the time integral of the square of the control input. Hence

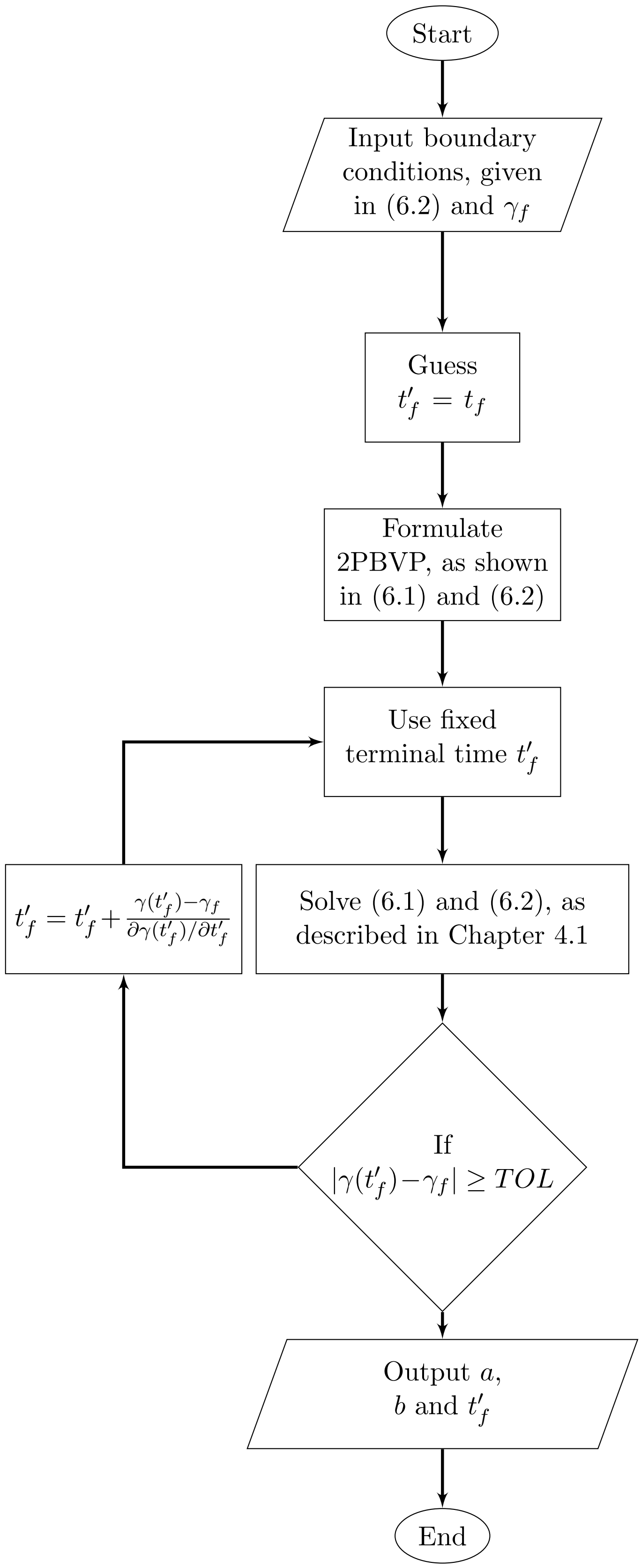

Figure 6.1: Block diagram for predictive time-linear control

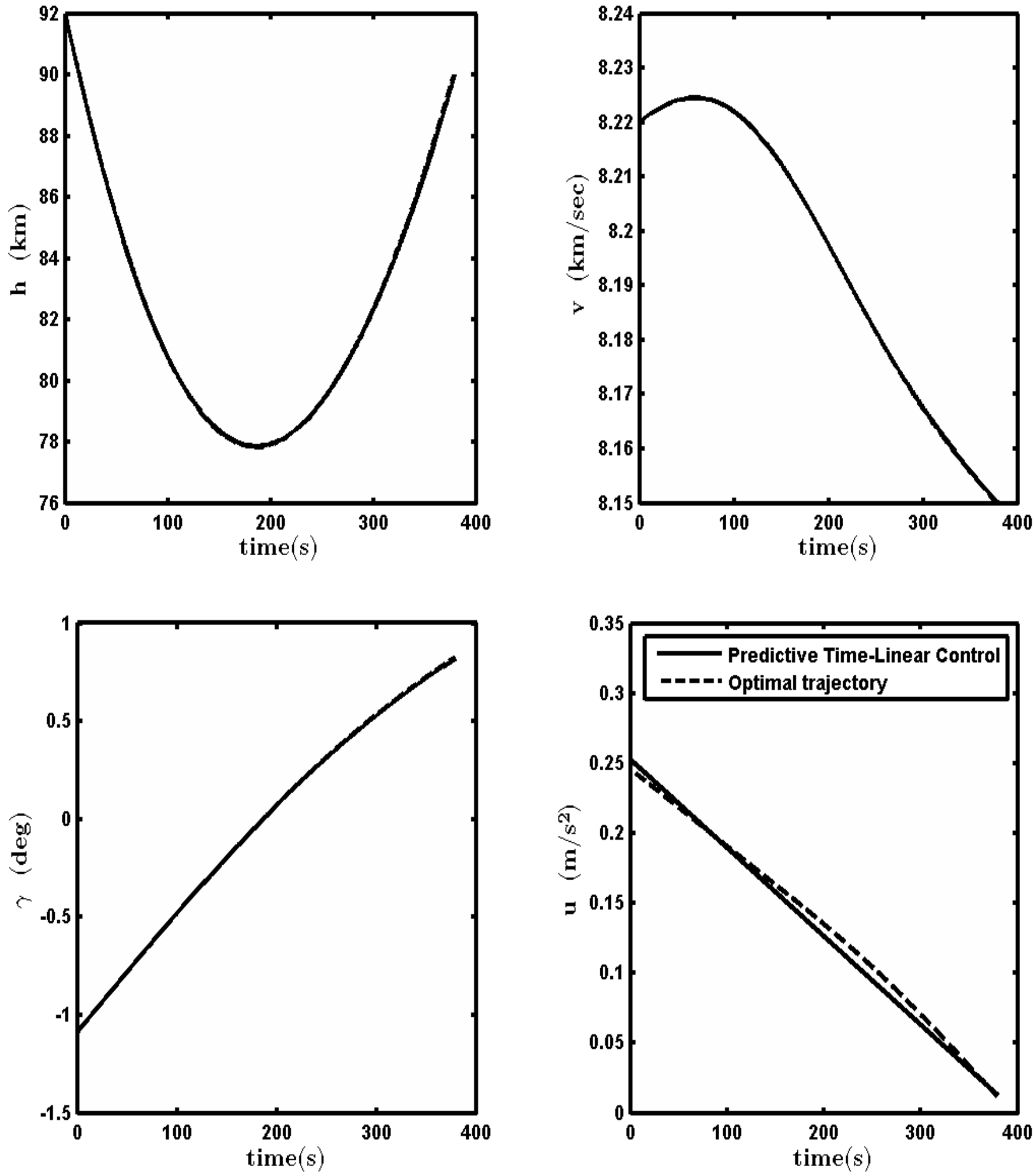

Figure 6.2: Comparison between the time-linear control and the optimal control trajectories

instead of using an optimal control law which is generally non-linear in nature, we can use a time-linear control law that helps satisfy all the six boundary conditions and at the same time also proves to be almost optimal. Fig. 6.3 presents the comparisons between the trajectories generated through time-linear control and the optimal trajectories for three different initial conditions and yet leading to the same exit conditions.

As discussed earlier, the time-linear control law requires only three parameters to be mentioned which are the control input at t=0 (a), the slope of the control input with respect to time (b) and the new final time (t'_f). In order to study the impact of the various perturbed initial conditions on the control profile, it is important to study the impact on these three parameters. Hence, an extensive study was done on the impact of the various perturbed initial altitudes on the three parameters a, b and t'_f with all the other boundary conditions staying unchanged. The same is repeated for variations in initial velocity and initial flight path angle. This analysis gives us an insight into the effect on the control profile due to the perturbed initial conditions and is presented in Figs. 6.4- 6.6.

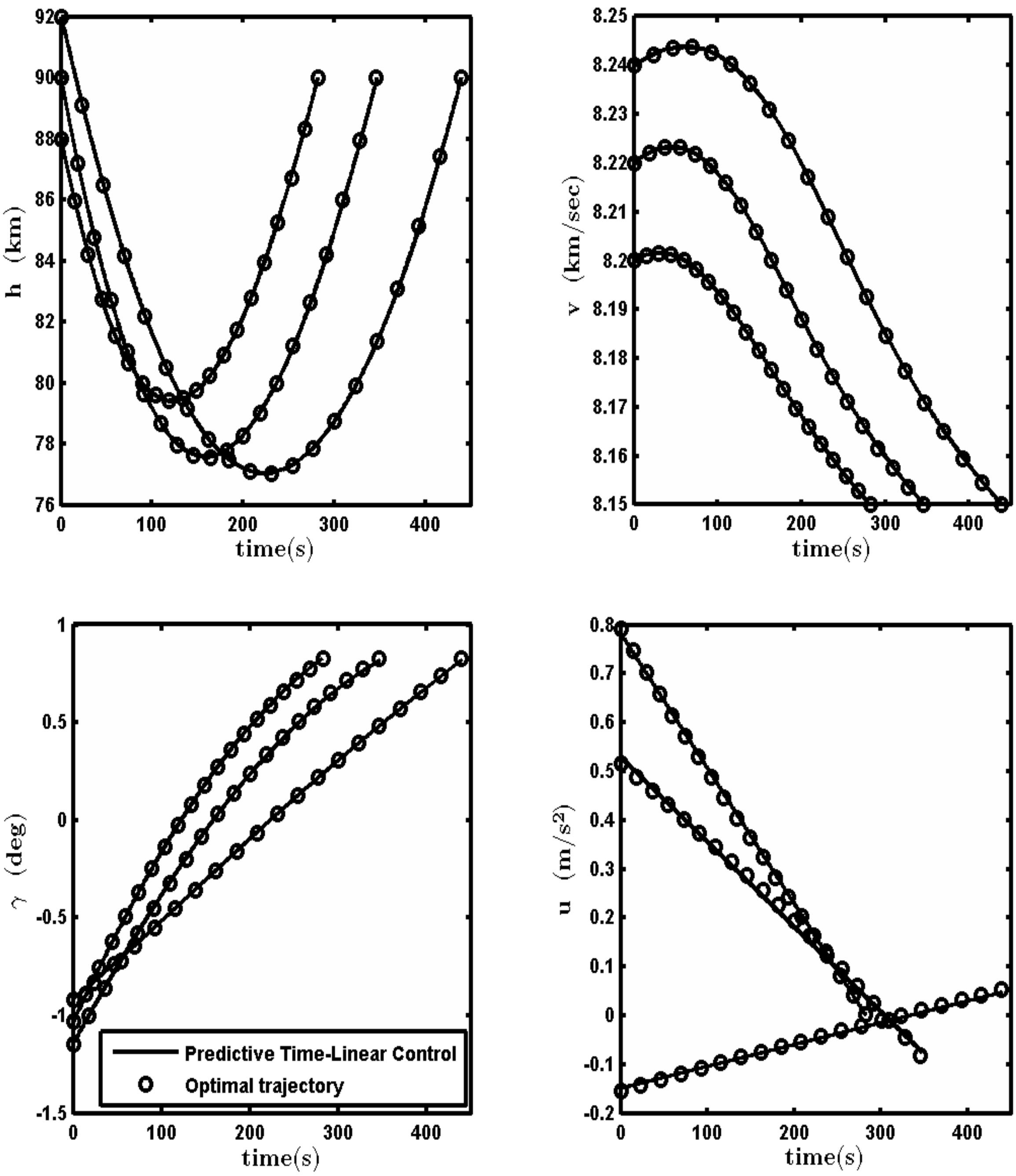

Figure 6.3: Comparison between the time-linear control and the optimal control trajectories for various perturbed initial conditions

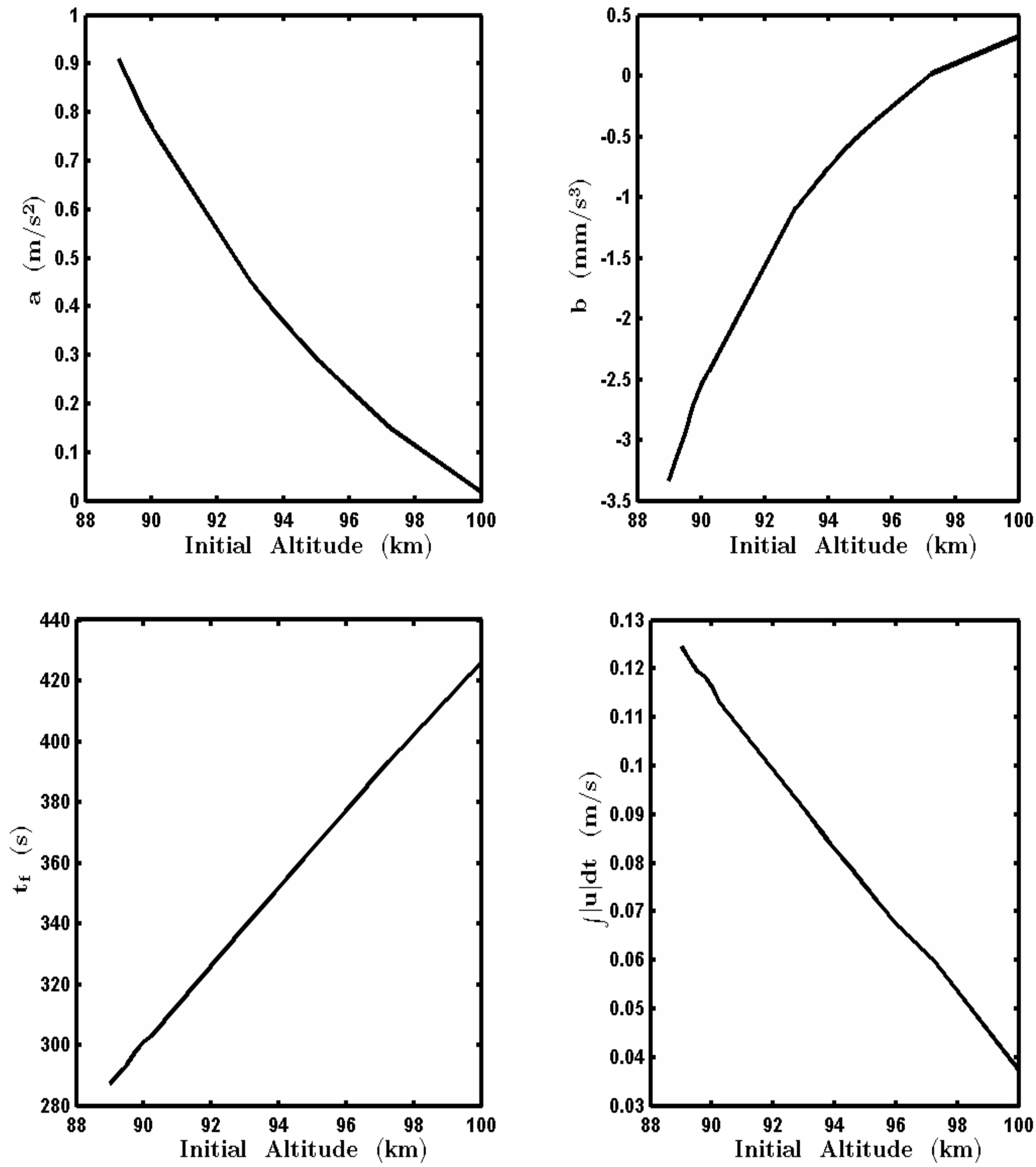

Figure 6.4: Variation of the three parameters a, b, t_f and the magnitude of the control effort with respect to the change in initial altitude

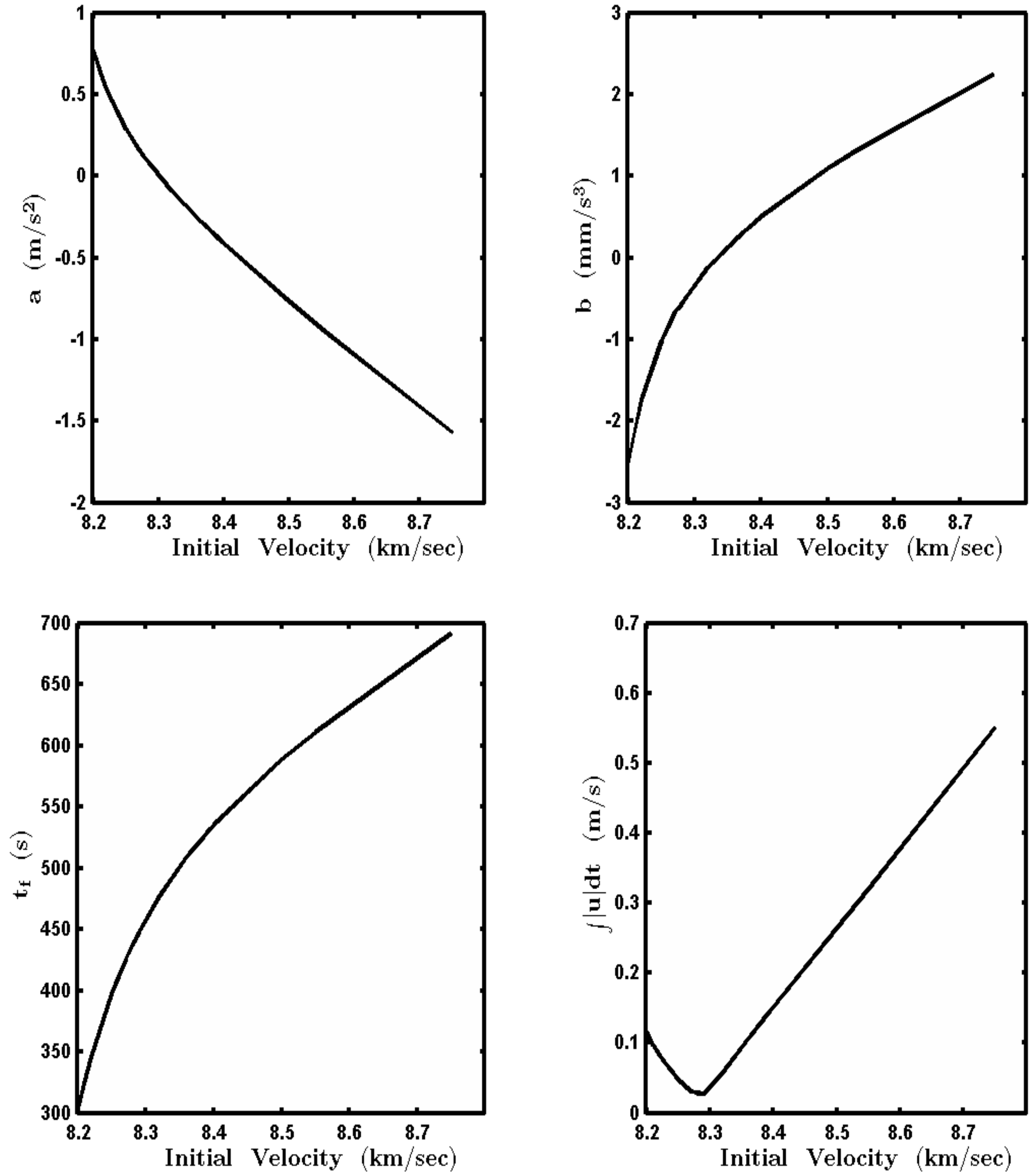

Figure 6.5: Variation of the three parameters a, b, t_f and the magnitude of the control effort with respect to the change in initial velocity

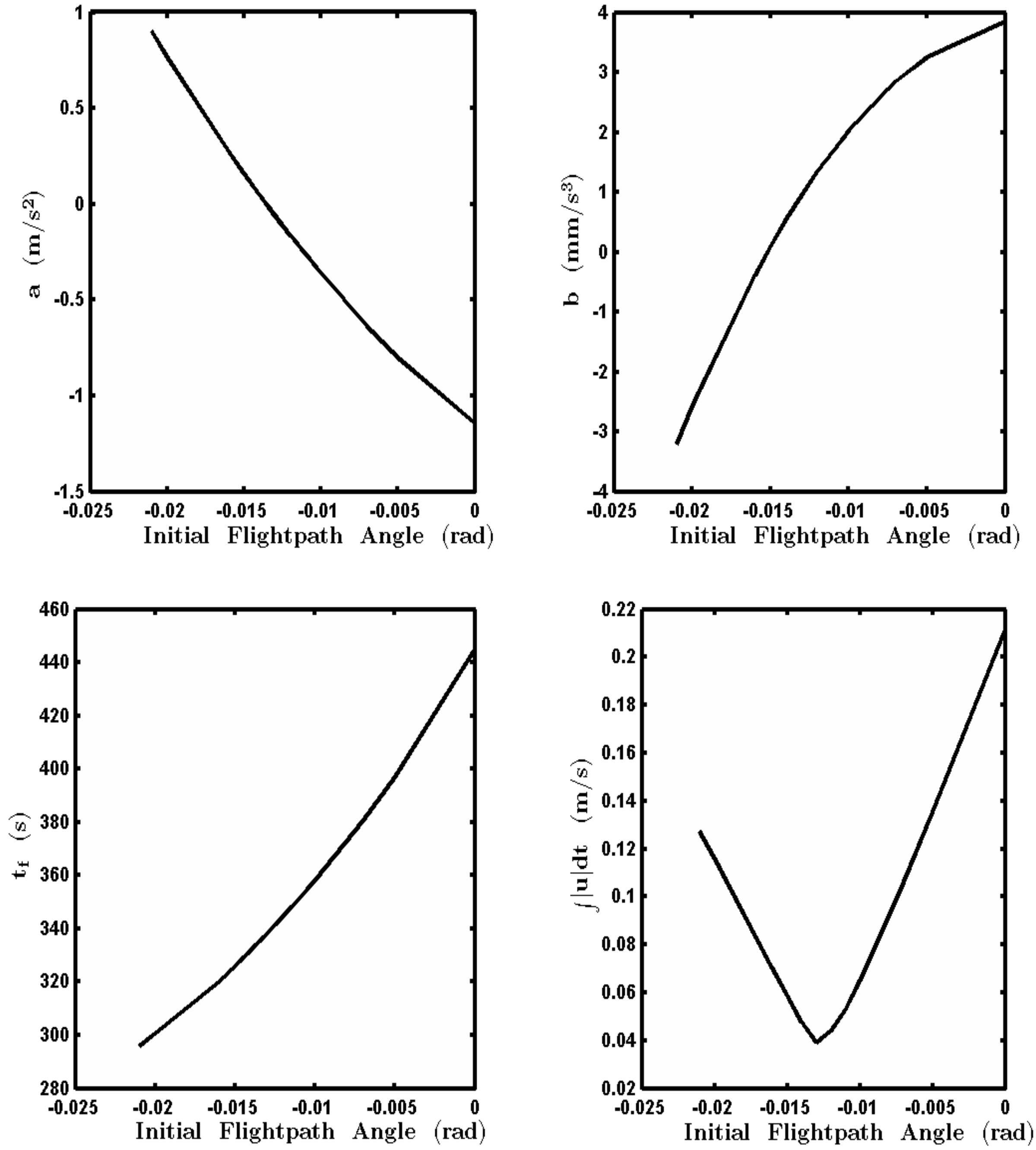

Figure 6.6: Variation of the three parameters a, b, t_f and the magnitude of the control effort with respect to the change in initial flight path angle

7

Robust Feedback Control

7.1 Robust Feedback Control

A robust feedback control law is obtained in order to compensate for the stochastic nature of the ballistic parameter which is modeled by randomly choosing a value about $\pm 20\%$ of the nominal value, used upto this point. In order to be able to obtain a control law that could give a satisfactory response, it is important to revisit the plant state equations from (2.7) and investigate the impact of the control input on various state variables. While the stochastic nature of the drag coefficient impacts mainly the velocity, the control input is applied to control the flight path angle and through that control velocity and altitude. Upon inspecting the state equation for the flight path angle we can conclude that the rate of change of flight path angle has a linear dependence on the ratio of control input (u) and velocity (v). Considering a linear feedback control with constant gains for the error terms corresponding to altitude and velocity while the gain corresponding to error in flight path angle is taken directly proportional to the velocity of the vehicle. The feedback control input for the robust feedback control is represented by Δu, while the errors in the radial distance, velocity and flight path angle are given by Δr, Δv and $\Delta\gamma$. Equation (7.1) gives the feedback control input for the system.

$$\Delta u = -\kappa_r \Delta r - \kappa_v \Delta v - \kappa_\gamma \Delta\gamma \tag{7.1}$$

$$\text{where,} \tag{7.2}$$

$$\kappa_r = 1.086957 \times 10^{-4} \tag{7.3}$$

$$\kappa_v = 6.082725 \times 10^{-2} \tag{7.4}$$

$$\kappa_\gamma = 0.526 v_m \tag{7.5}$$

It can be observed from Fig. 7.1 that the errors in all the three states are diverging away from the zero error line when there is no feedback, while they converge to a value closer to zero when the robust feedback control system is deployed. On the other hand, Fig. 7.2 presents a comparison between the nominal trajectory which is an ideal case where there is no uncertainty in ballistic parameter with various trajectories where the stochastic nature of the ballistic parameter is compensated using the robust controller. It can be observed that the robust controller with linear feedback provides satisfactory

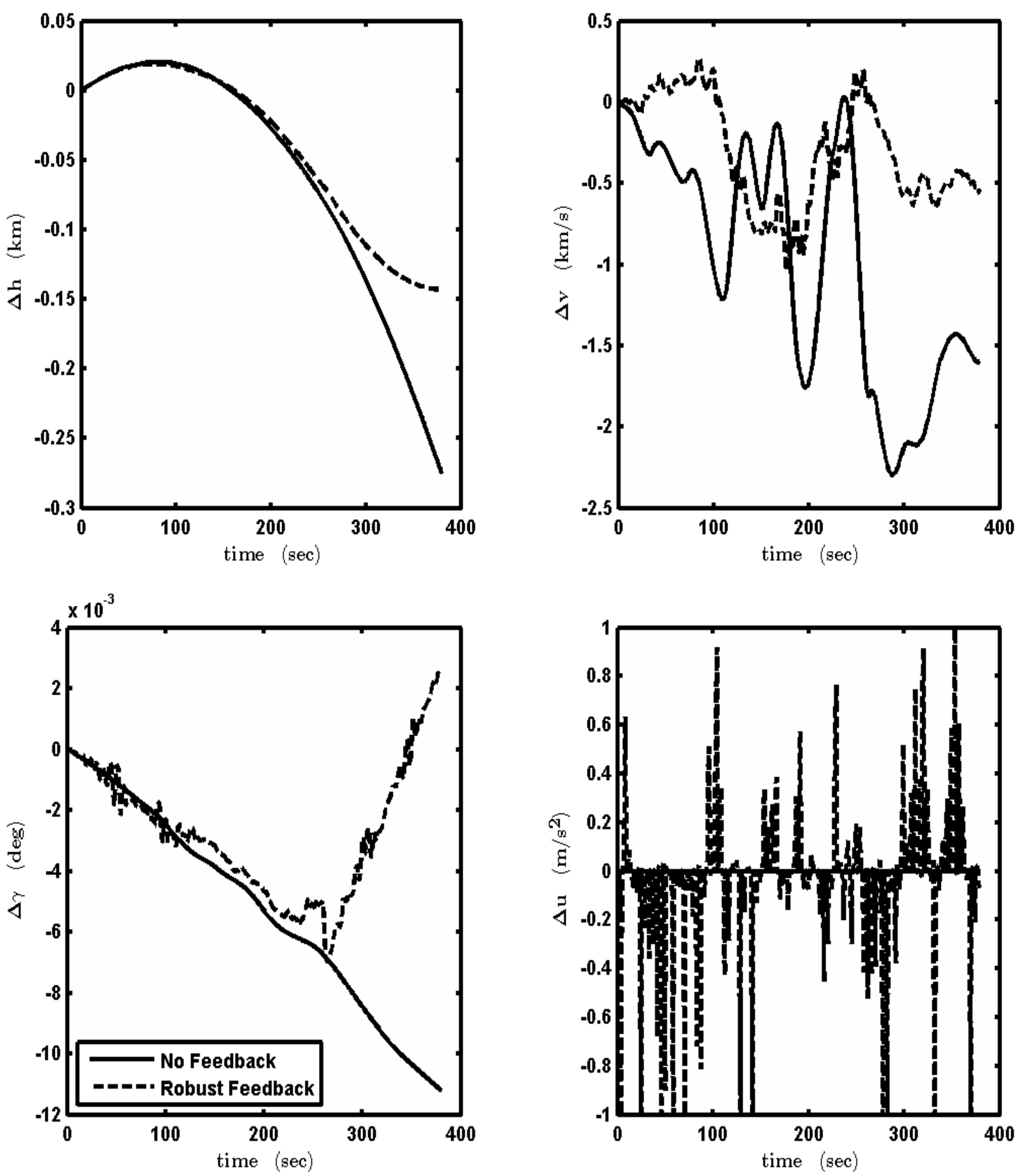

Figure 7.1: The errors in states and adaptive control input for the case using robust controller as compared to the one without

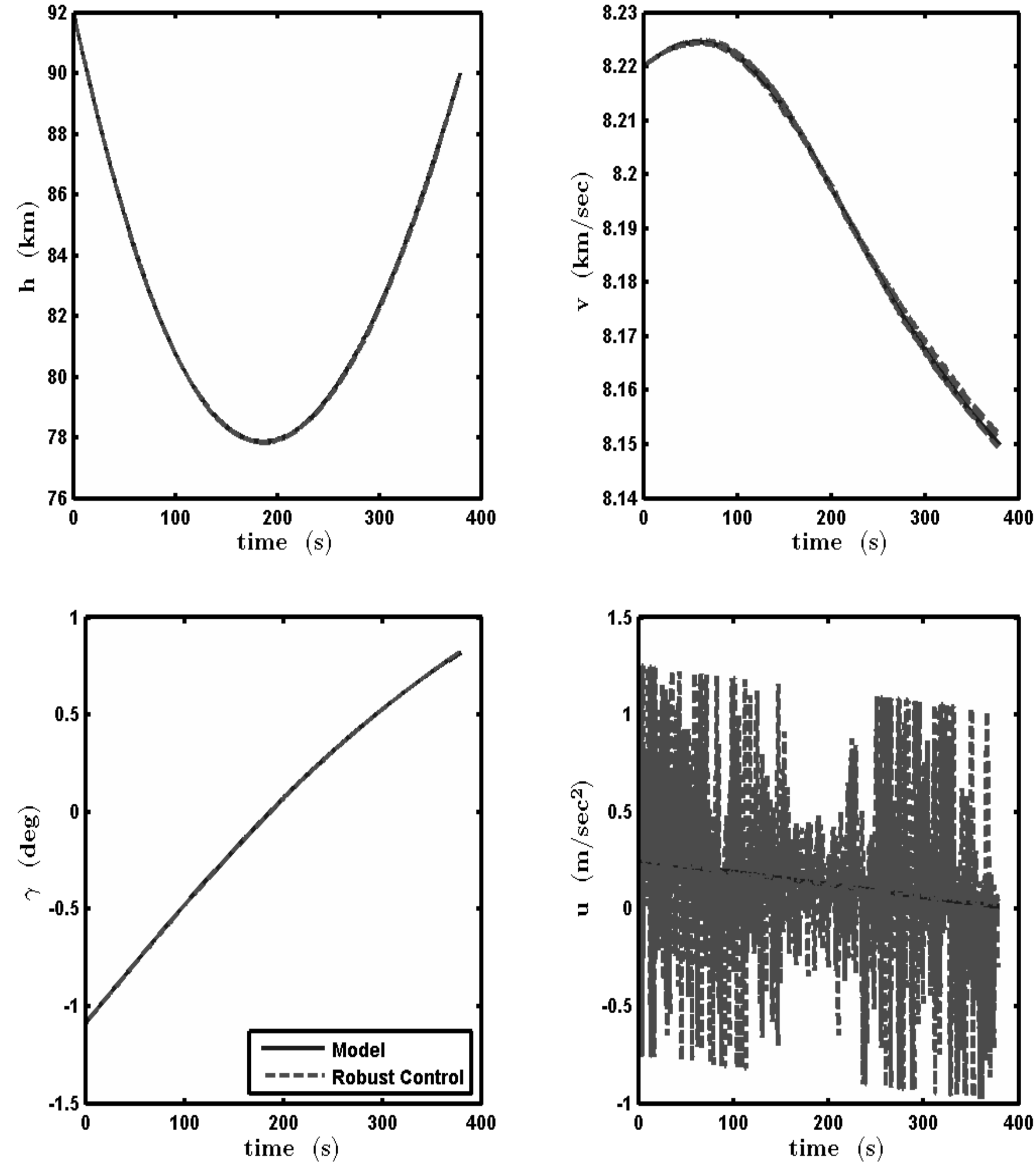

Figure 7.2: Comparison between the nominal trajectory and various test cases of trajectories using robust controller

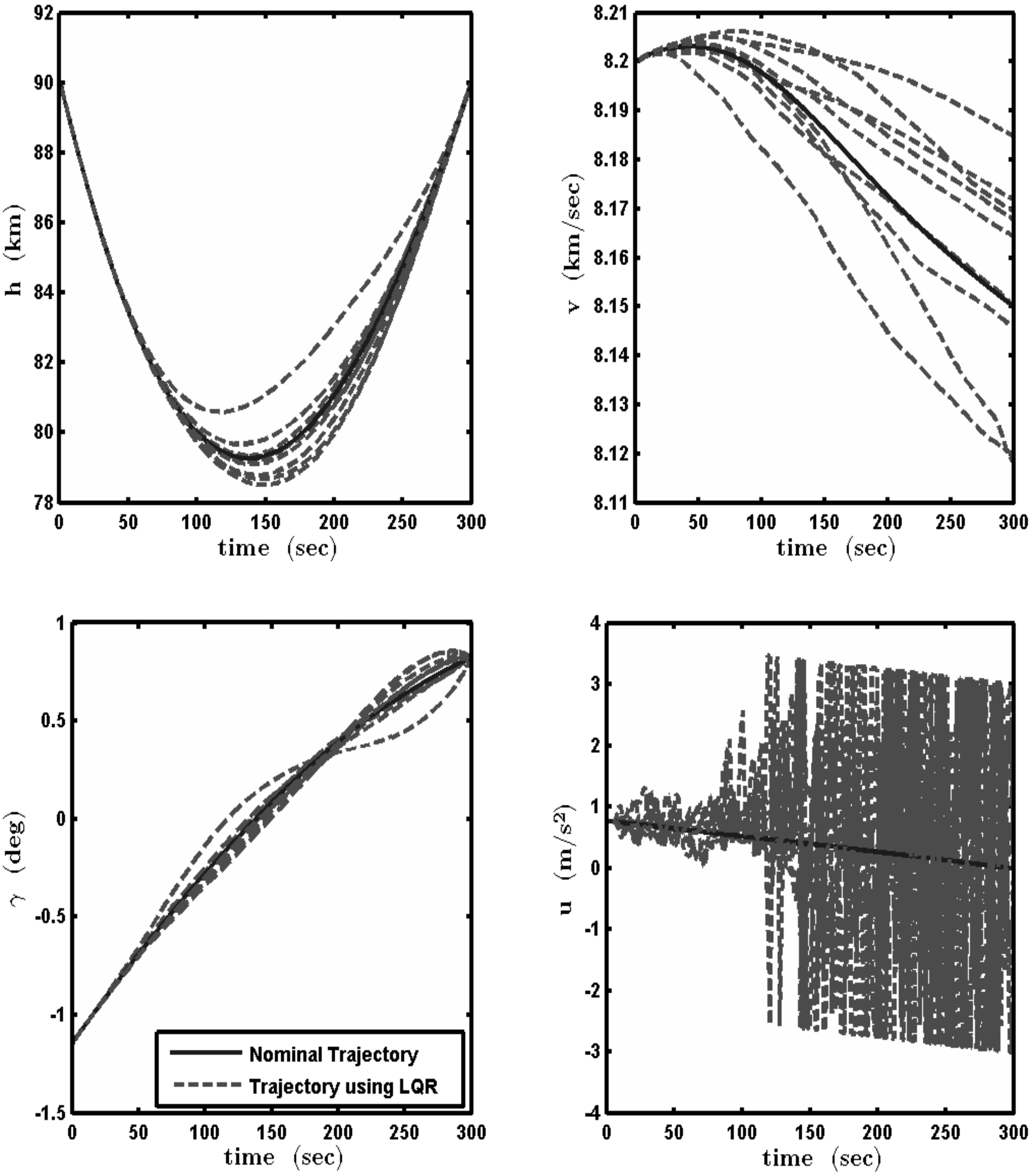

Figure 7.3: Comparison between the nominal trajectory and various test cases of trajectories using terminal time LQR

performance. In order to be able to appreciate the simplicity and superiority of this scheme, a terminal time LQR presented in chapter 5.2 is used to compensate for the stochastic nature of the ballistic parameter and the results are presented in Fig. 7.3.

8

Adaptive Control

Predictive time-linear control methodology discussed in chapter 6 deals with adjusting the slope, initial control input and final time of a nominal time-linear control input to account for deviations in initial conditions. This methodology assumes a specific model for the plant defined by certain parameters to develop the new time-linear control law which would be effective only under the assumption that these parameters don't change. The parameters for this model are acceleration due to gravity (g) and the ballistic parameter (K). The change in acceleration due to gravity over the small range of altitudes involved in an aeroassist maneuver can be safely neglected, while it is important to investigate the constituent terms in the ballistic parameter to comment on its nature.

8.1 Predictive Adaptive Control

The base density of the atmospheric model assumed may not necessarily be the expected one and it is not possible to estimate the exact value of C_{D_0} before reentry, having a different value for the ballistic parameter would lead to different exit conditions as compared to the desired ones. If this change in ballistic parameter is known a priori, it is possible to use this new value of K in the predictive time-linear control model and obtain the values of a, b and t'_f such that the exit conditions are met. An analysis on the predictive time-linear control law is done for a range of values about the nominal value of the ballistic parameter assumed is presented in Table 8.1. The ballistic parameter can be estimated at reentry using

$$K = -\left(\frac{\dot{v} + gsin\gamma_0}{\exp^{-h_0/H} v_0^2}\right) \tag{8.1}$$

where, $\dot{v}$ can be measured using accelerometers. If this value of K turns out to be different from the one assumed in the predictive time-linear control method, it would lead to a different exit condition. Based on the information given in the Table 8.1, plots were made to show the variation of a, b and t_f with respect to the ballistic parameter K and given in Fig. 8.1. It can be observed that the variation of a, b and t_f with respect to K is linear, which is very helpful as a straight line can be fitted through the data and an empirical expression is obtained given in Eq. (8.2)- (8.4).

Table 8.1: Ballistic parameter variation

Ballistic Parameter (1/m)	$a \quad (m/s^2)$	$b \quad (m/s^3)$	$t_f \quad (s)$	$\int \lvert u \rvert dt \quad (km/s)$
0.0002336	0.633419201	-0.002032061	332.2244687	0.099148864
0.00024	0.650203935	-0.002105412	327.9266633	0.100782653
0.00025	0.672450161	-0.002173017	322.6315003	0.104234172
0.00026	0.700237749	-0.002317169	315.7716585	0.106015604
0.00027	0.719831922	-0.002358413	311.6257794	0.109901126
0.000292	0.769349796	-0.002546601	300.9622284	0.116211703
0.0003	0.789657293	-0.002651214	296.6114613	0.117596641
0.00031	0.813292134	-0.00276172	291.7738226	0.119741458
0.00032	0.832813066	-0.002818261	288.1658147	0.122973347
0.00033	0.855070656	-0.002916361	283.9241124	0.12522635
0.000335	0.868977731	-0.003006461	281.1239682	0.125488569

$$a\ (\mathrm{m/s^2}) = 2.32306K + 0.090752 \tag{8.2}$$

$$b\ (\mathrm{m/s^3}) = (-8.99571K + 0.0623299) \times 10^{-3} \tag{8.3}$$

$$t_f\ (\mathrm{s}) = -503.94971K + 448.94712 \tag{8.4}$$

It is important to note that, as the value of the ballistic parameter is increased we can observe a gradual reduction in final time which is intuitive. The increase in ballistic parameter can be perceived in terms of a higher base density for the atmospheric model assumed, which would also mean that the AOT vehicle can be decelerated faster and thus would require to spend lesser amount of time inside the atmosphere. The comparison between the case where the nominal value for ballistic parameter is used and the case where a perturbed one is used, is presented in Fig. 8.2. It can be observed that the reentry and exit conditions remain the same, while the two trajectories follow different paths. This depicts the role of ballistic parameter in shaping the predictive time-linear control trajectory. This method can be implemented onboard but offline,

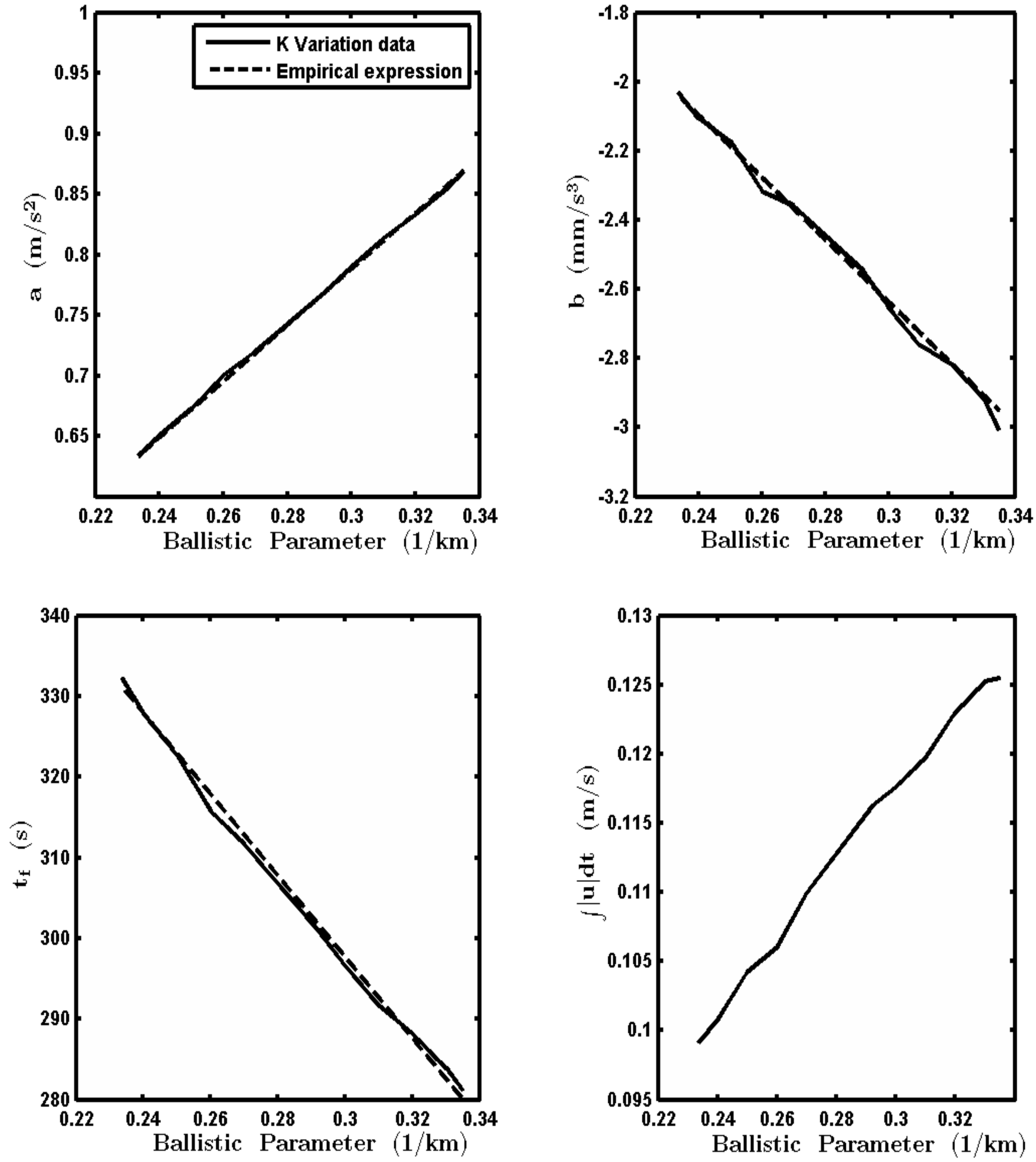

Figure 8.1: Variation of a, b and t_f with respect to the ballistic parameter K and comparison with the empirical expression

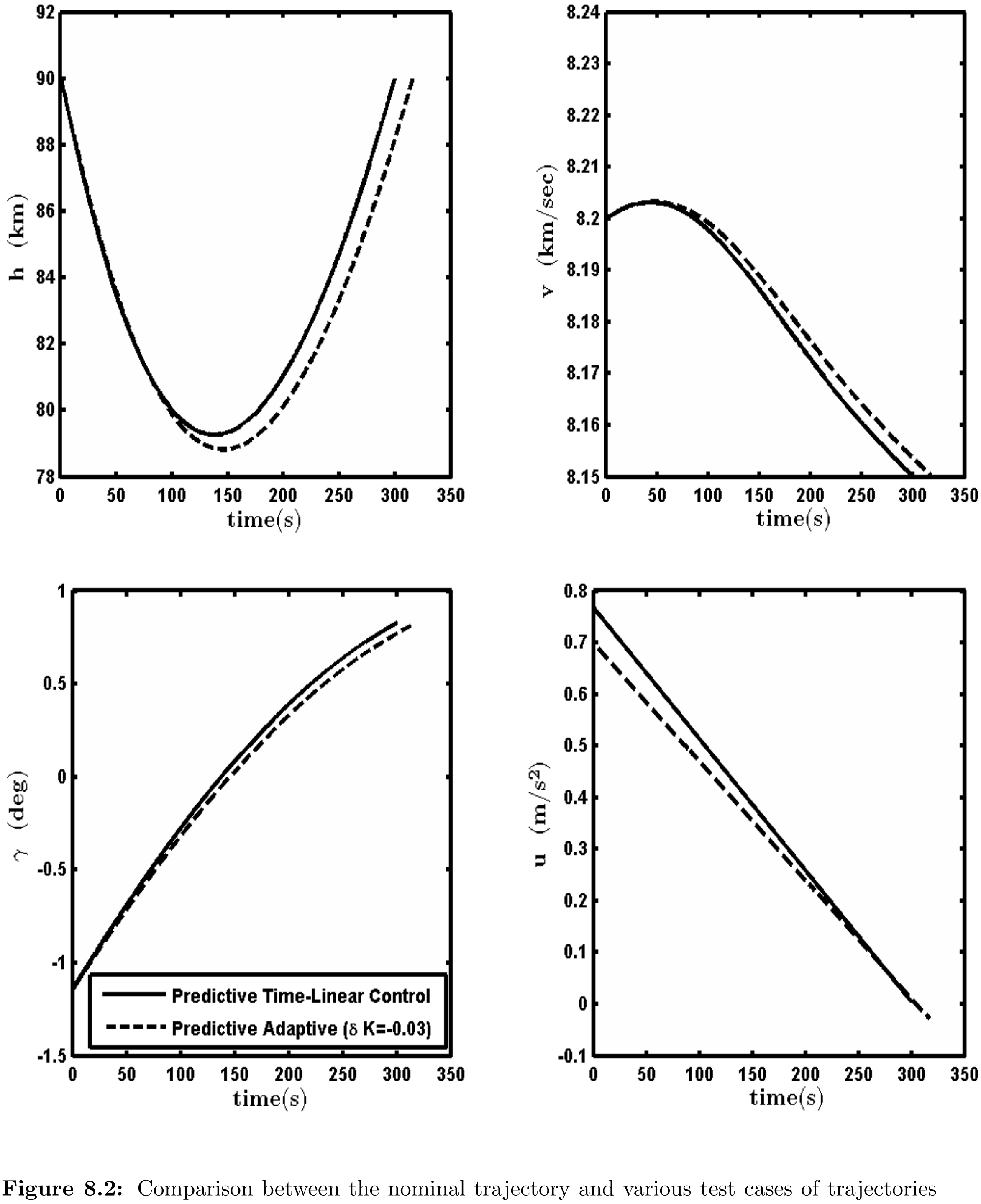

Figure 8.2: Comparison between the nominal trajectory and various test cases of trajectories using adaptive controller

hence real time adaptation is not a viable option due to the long times involved in computation. Hence, there is a need to develop a feedback adaptive control system to handle real time changes in the ballistic parameter.

8.2 Real-time Feedback Adaptive Control

By inspecting the constituent terms involved in the expression for ballistic parameter from (**??**), we can conclude that C_{D_0} may not necessarily be constant throughout the maneuver as it depends on Mach Number and the effect of shock on the magnitude of the coefficient of drag may vary from one angle of attack to another.

8.2.1 Formulation

In order to incorporate this change in ballistic parameter into the system, a $\pm 20\%$ uncertainty is introduced which needs to be compensated by the adaptive control system. In order to do so, the following proposition is suggested,

Proposition. *Let* $\mathbf{e} \in \mathbb{R}^3$ *and* $\Delta u \in \mathbb{R}$ *be the error in the states and the control input required for the linearized state equations given by,*

$$\dot{\mathbf{e}} = A\mathbf{e} + B\Delta u \tag{8.5}$$

where A *and* B *are given by* (5.2) *and* (5.3). *Factoring the stochastic nature of* K, *it is assumed that* A *is not entirely deterministic. Let the control law employed be a*

Proportional-Differential (PD) one and be given by,

$$\Delta u = -\eta \Theta^T \mathbf{e} - \Psi \Theta^T \dot{\mathbf{e}} \tag{8.6}$$

where, $\Theta \in \mathbb{R}^3$ be the adaptation gain vector, $\eta \in \mathbb{R}$ and $\Psi \in \mathbb{R}$ are the proportional and differential design constants to be chosen. Considering the Lyapunov function,

$$V = \frac{\Phi}{2} \mathbf{e}^T P \mathbf{e} + (\Theta - \Theta_0)^T (\Theta - \Theta_0) \tag{8.7}$$

where, $\Phi \in \mathbb{R}$ is a positive adaptation constant and P is a symmetric positive definite coefficient matrix. Then, the adaptive control law

$$\Delta u = -\Theta^T \left(\frac{\eta I + \Psi A}{1 + \Psi \Theta^T B} \right) \mathbf{e} \tag{8.8}$$

and the adaptation law

$$\dot{\Theta} = \frac{\eta \Phi}{1 + \Psi \Theta^T B} (\mathbf{e} B^T P \mathbf{e}) \tag{8.9}$$

are proven to exhibit asymptotic stability.

Proof. *Substituting* (8.5) *in* (8.6), *we get*

$$\Delta u = -\eta \Theta^T \mathbf{e} - \Psi \Theta^T (A\mathbf{e} + B\Delta u) \tag{8.10}$$

$$(1 + \Psi \Theta^T B)\Delta u = -\Theta^T (\eta I + \Psi A)\mathbf{e} \tag{8.11}$$

$$\Delta u = -\Theta^T \left(\frac{\eta I + \Psi A}{1 + \Psi \Theta^T B} \right) \mathbf{e} \tag{8.12}$$

Substituting (8.12) *in* (8.5),

$$\dot{\mathbf{e}} = A\mathbf{e} - B\Theta^T \left(\frac{\eta I + \Psi A}{1 + \Psi \Theta^T B} \right) \mathbf{e} \tag{8.13}$$

$$\dot{\mathbf{e}} = \left(\left(I - \frac{\Psi B \Theta^T}{1 + \Psi \Theta^T B} \right) A - \frac{\eta B \Theta^T}{1 + \Psi \Theta^T B} \right) \mathbf{e} \tag{8.14}$$

Let,

$$A_m = \left(I - \frac{\Psi B \Theta^T}{1 + \Psi \Theta^T B} \right) A - \frac{\eta B \Theta_0^T}{1 + \Psi \Theta^T B} \tag{8.15}$$

$$\implies A = \left(I - \frac{\Psi B \Theta^T}{1 + \Psi \Theta^T B} \right)^{-1} \left(A_m + \frac{\eta B \Theta_0^T}{1 + \Psi \Theta^T B} \right) \tag{8.16}$$

where,

$$A_m = \begin{pmatrix} 0 & sin\gamma_d & v_d cos\gamma_d \\ 0 & -2K\, exp^{-(r_{avg} - R_e)/H} v_d & -g cos\gamma_d \\ -v_d/{r_d}^2 & \left(\frac{1}{r_d} + \frac{g}{{v_d}^2} \right) cos\gamma_d - \frac{u_d}{{v_d}^2} & -\left(\frac{v_d}{r_d} - \frac{g}{v_d} \right) sin\gamma_d \end{pmatrix} \tag{8.17}$$

Substituting (8.16) *in* (8.14),

$$\dot{\mathbf{e}} = \left(A_m - \frac{\eta B(\Theta - \Theta_0)^T}{1 + \Psi\Theta^T B} \right) \mathbf{e} \tag{8.18}$$

Differentiating the Lyapunov function in (8.19) *with respect to time, we get*

$$\dot{V} = \frac{\Phi}{2}\dot{\mathbf{e}}^T P \mathbf{e} + \frac{\Phi}{2}\mathbf{e}^T P \dot{\mathbf{e}} + (\Theta - \Theta_0)^T \dot{\Theta} \tag{8.19}$$

Substituting (8.18) *in* (8.19) , *we have*

$$\dot{V} = \frac{\Phi}{2}\mathbf{e}^T (A_m^T P + P A_m)\mathbf{e} - \frac{\Phi}{2}(\Theta - \Theta_0)^T 2\nu \left(\frac{\mathbf{e} B^T P \mathbf{e}}{1 + \Psi\Theta^T B} \right) + (\Theta - \Theta_0)^T \dot{\Theta} \tag{8.20}$$

From continuous Lyapunov equation [18], we have

$$A_m^T P + P A_m = -Q \tag{8.21}$$

where Q *is positive definite, if* P *is positive definite and* A_m *is asymptotically stable.* A_m *being time-varying matrix, can be proven to be exponentially stable using the sufficient conditions for stability of linear time-varying systems [19]. These sufficient conditions require all the eigen values of* A_m *to be negative from* t_0 *to* t_f *and the* $||\dot{A}_m|| \leq \delta$ *provided* $\delta > 0$ *is sufficiently small. From Fig. 8.3, it can be observed that all the three eigen values of* A_m *are negative and the norm of* $\dot{A}_m$ *is bounded. Using* (8.21) *in* (8.20), *we*

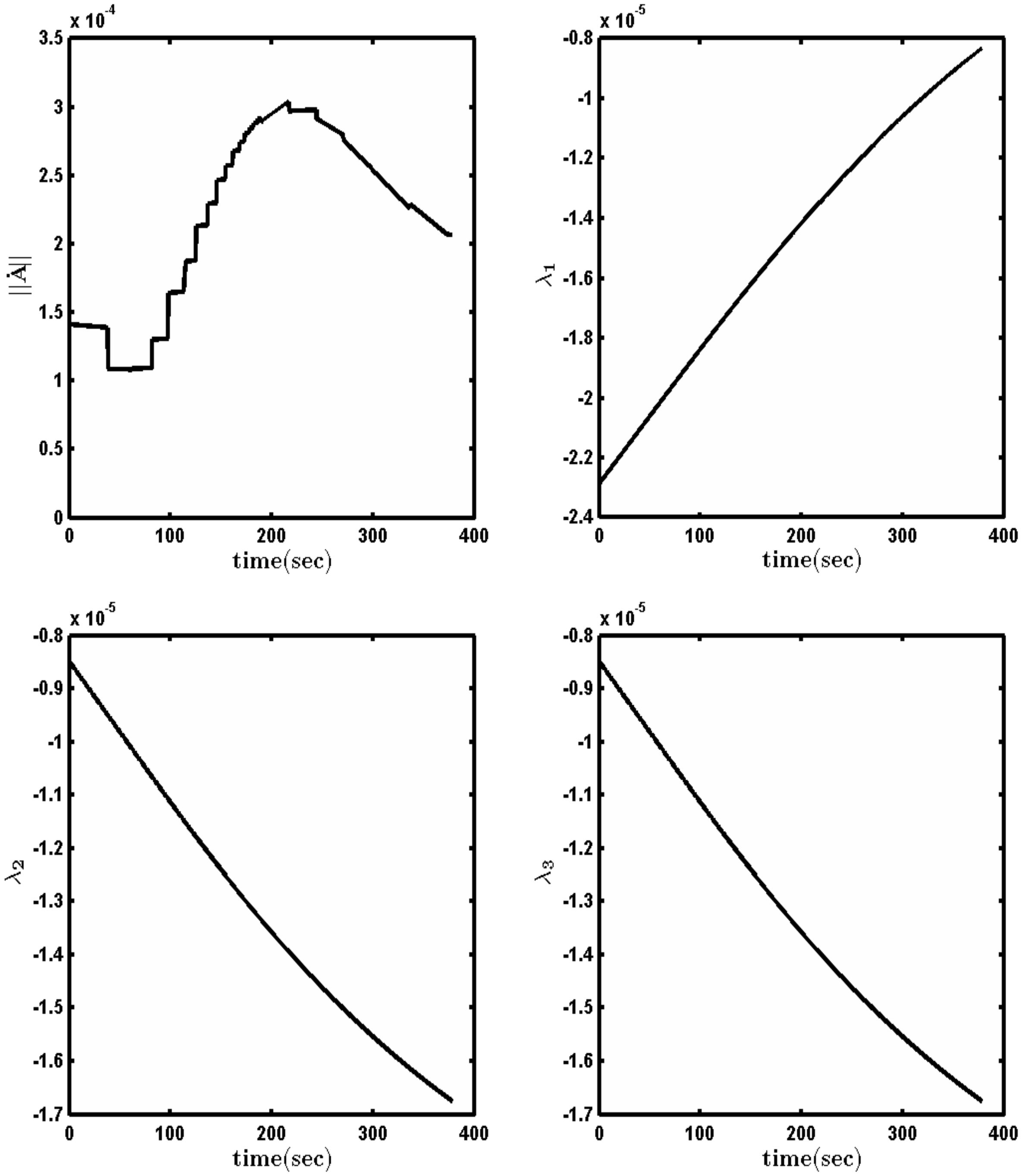

Figure 8.3: The variation of the three eigen values of A_m and the norm of $\dot{A}_m$ with respect to time

have

$$\dot{V} = -\frac{\Phi}{2}\mathbf{e}^T Q\mathbf{e} + (\Theta - \Theta_0)^T\left(\dot{\Theta} - \left(\frac{\eta\Phi}{1 + \Psi\Theta^T B}\right)\mathbf{e}B^T P\mathbf{e}\right) \tag{8.22}$$

Let,

$$\dot{\Theta} = \left(\frac{\eta\Phi}{1 + \Psi\Theta^T B}\right)\mathbf{e}B^T P\mathbf{e} \tag{8.23}$$

From (8.22) *and* (8.23), *we have*

$$\dot{V} = -\frac{\Phi}{2}\mathbf{e}^T Q\mathbf{e} \tag{8.24}$$

From Equation (8.21), Q *is positive definite and* Φ *is a positive number. This would make,*

$$\dot{V} < 0 \tag{8.25}$$

From Equation (8.25) *and the Lyapunov theorem for stability [18], it can be concluded that the system* (8.5) *using the control law* (8.8) *and the adaptation law* (8.9) *exhibits asymptotic stability.*

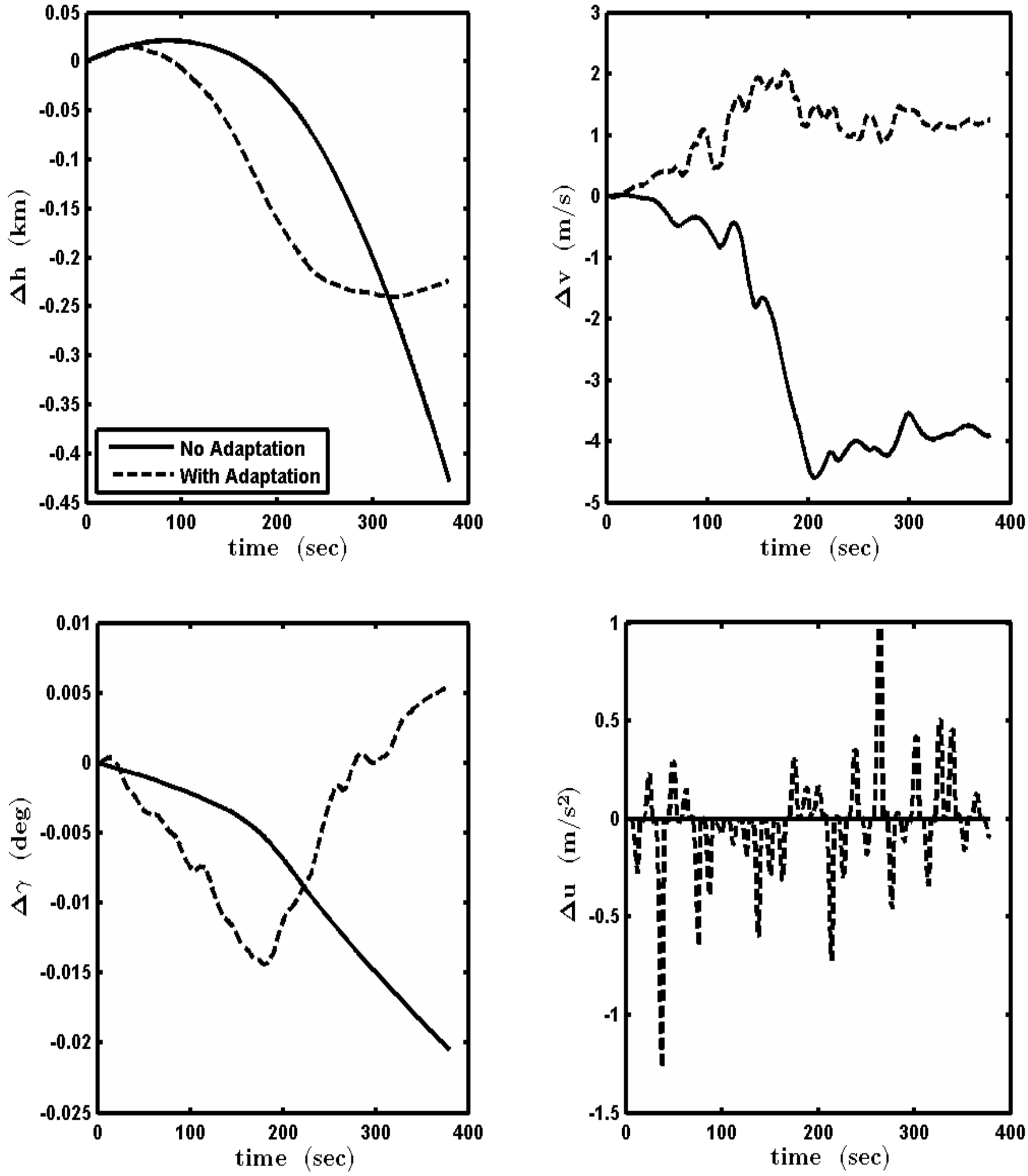

Figure 8.4: The errors in states and adaptive control input for the case with adaptation as compared to the one without

8.2.2 Implementation

The adaptive control methodology formulated above is implemented on the system given by (2.7) to compensate for the uncertainty involved in estimating C_{D_0} (ballistic parameter, K). For this adaptive control problem, $\mathbf{e} = \{\Delta h \quad \Delta v \quad \Delta\gamma\}^T$ and $\Theta = \{\theta_h \quad \theta_v \quad \theta_\gamma\}^T$ with $\Phi = 1$, $\eta = 0.1$, $\Psi = 0.1$, $\Theta_0 = \{8.696 \times 10^{-3} \quad 54.745 \quad 526.316\}^T$ and

$$P = \begin{pmatrix} 0.1 & 0 & 0 \\ 0 & 0.05 & 0 \\ 0 & 0 & 10 \end{pmatrix}$$

Using the above design constants, an adaptive control system is implemented and a comparison is presented between the case with adaptation and the one without in Fig. 8.4. It can be clearly observed that the error in altitude and flight path angle diverge from the zero error line when there is no adaptation while they settle to a value closer to zero with adaptation. In the case of error in velocity, the adaptive controller ensures that the error settles to a value closer to the zero error line as compared to the case where there is no adaptation. In order to exhibit the effectiveness of the adaptive control methodology, a comparison between the nominal trajectory which is an ideal case with no uncertainty in ballistic parameter with various trajectories using the adaptive controller to compensate for the stochastic nature in ballistic parameter is

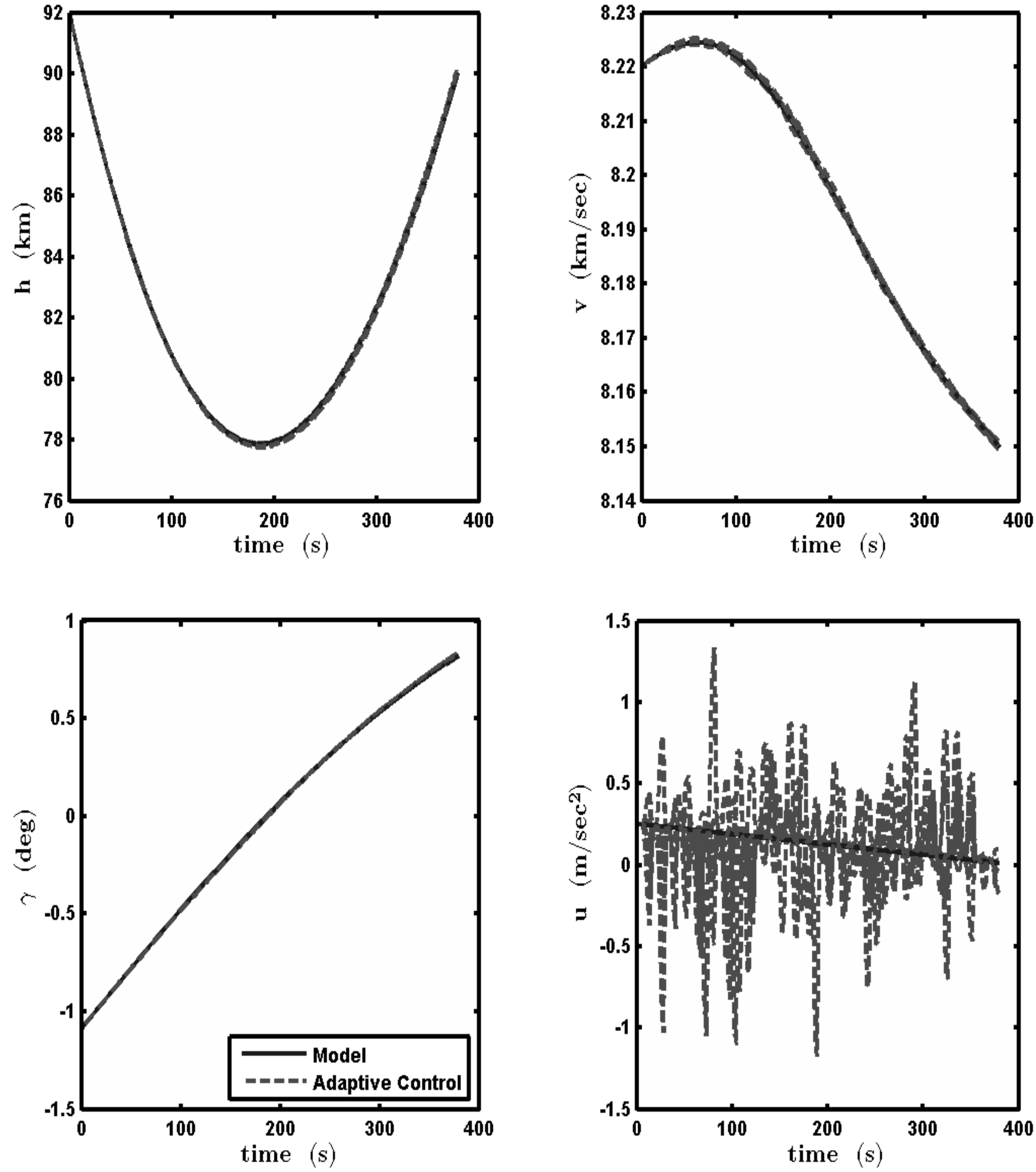

Figure 8.5: Comparison between the nominal trajectory and various test cases of trajectories using adaptive controller

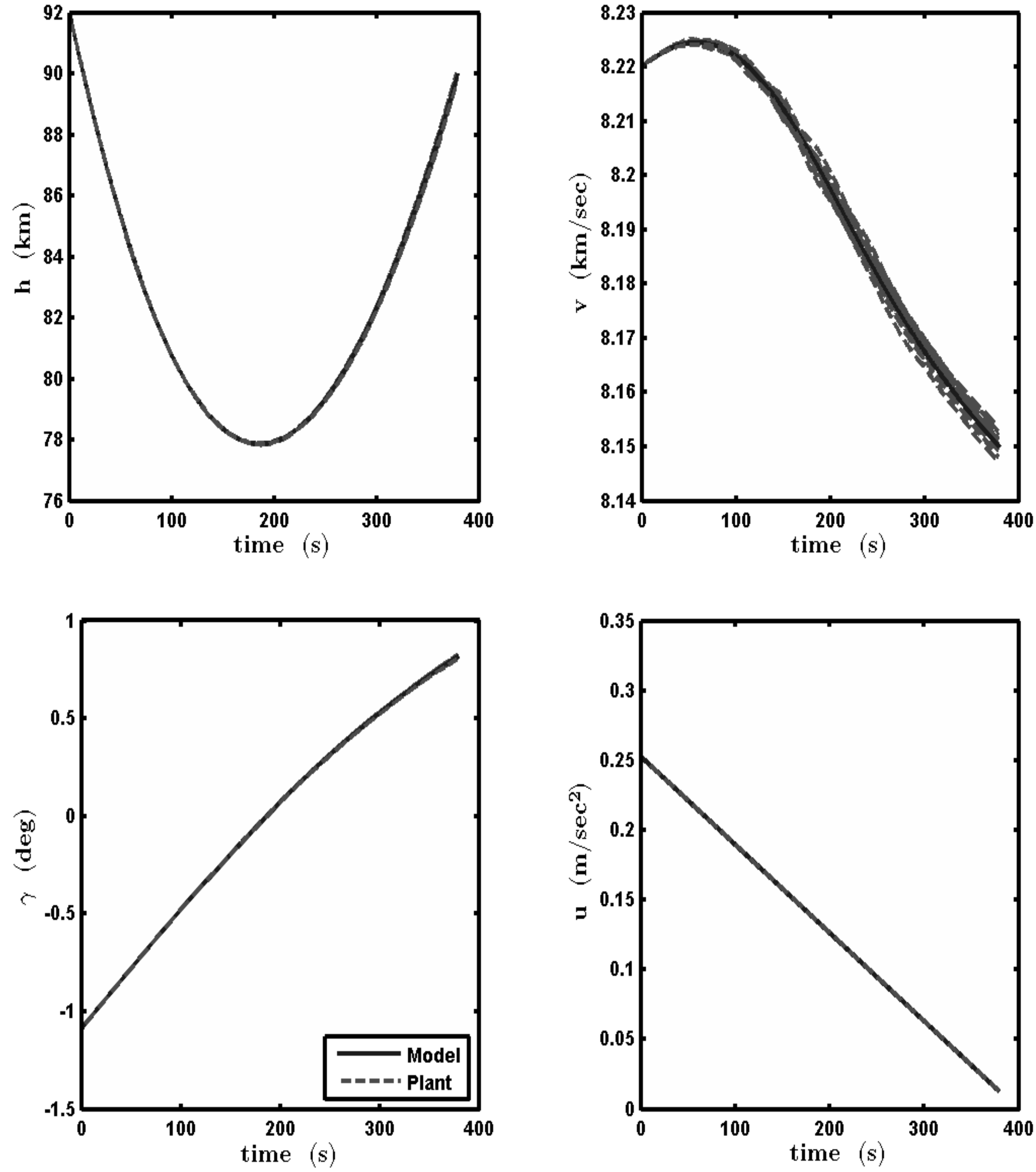

Figure 8.6: Comparison between the nominal trajectory and various test cases of the stochastic plant response with no adaptation

presented in Fig. 8.5. The performance of this adaptive controller can be appreciated by comparing it with Fig. 8.6 where no adaptation was used. It can also be observed that the adaptive control law has lesser chattering as compared to the robust feedback control law which would reduce the overall control effort considerably.

9

Review of the Scheme

At this point, it is important to revisit the complete mission plan for optimal aeroassisted orbital transfer. To start with, a deorbit impulse is applied at the circular HEO to instantly reduce the velocity of the spacecraft and put it into an elliptic transfer orbit with perigee altitude low enough to allow reentry into the Earth's atmosphere. As the spacecraft is approaching the Earth's atmosphere the reentry conditions are estimated and the predictive time-linear control methodology is used to obtain a near optimal time-linear control law. Just moments before reentry, the ballistic parameter is estimated using the accelerometer data and if it is found to be different from the one assumed in the predictive time-linear control, the empirical relation from predictive adaptive control is used to adjust the time-linear control profile to ensure the desired exit conditions are met. After entering the Earth's atmosphere, the real time adaptive controller is used to adapt to changes in the ballistic parameter and help meet

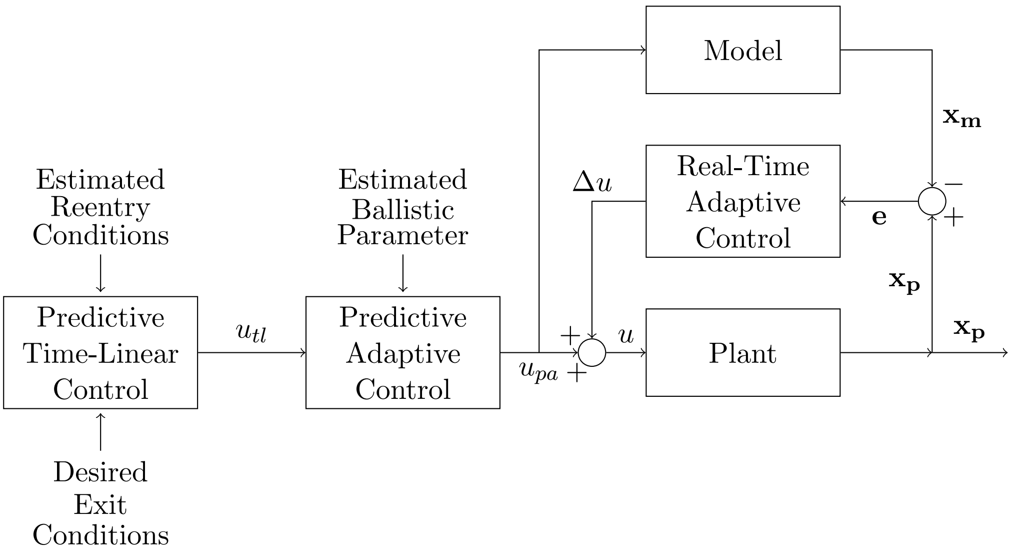

Figure 9.1: Block diagram for the suggested scheme

the desired exit conditions. After exiting the Earth's atmosphere with these desired conditions, a reorbit impulse is applied at the apogee of the transfer elliptical orbit. Thus putting the spacecraft into the desired circular LEO. The timeline for the entire mission is presented in Fig. 9.3.

The block diagrams for the suggested scheme using a combination of predictive time-linear, predictive adaptive and real time adaptive control methodologies is presented and compared with the existing scheme using a combination of optimal trajectory planning and robust control methodologies in Fig. 9.1 and 9.2.

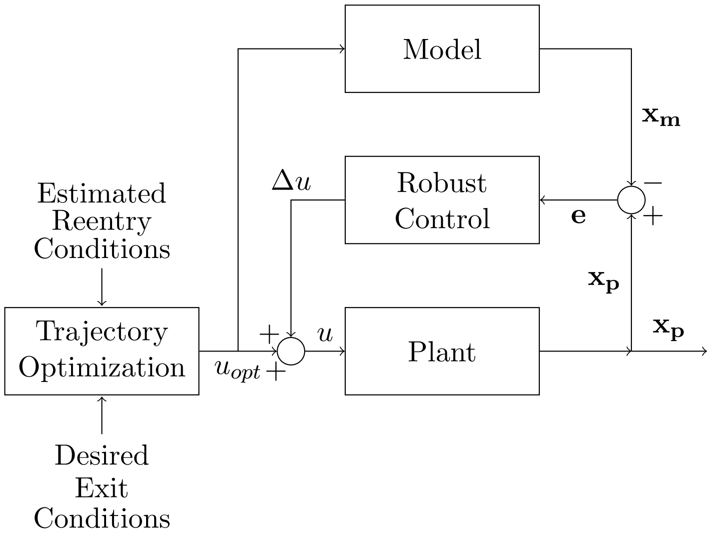

Figure 9.2: Block diagram for the existing scheme

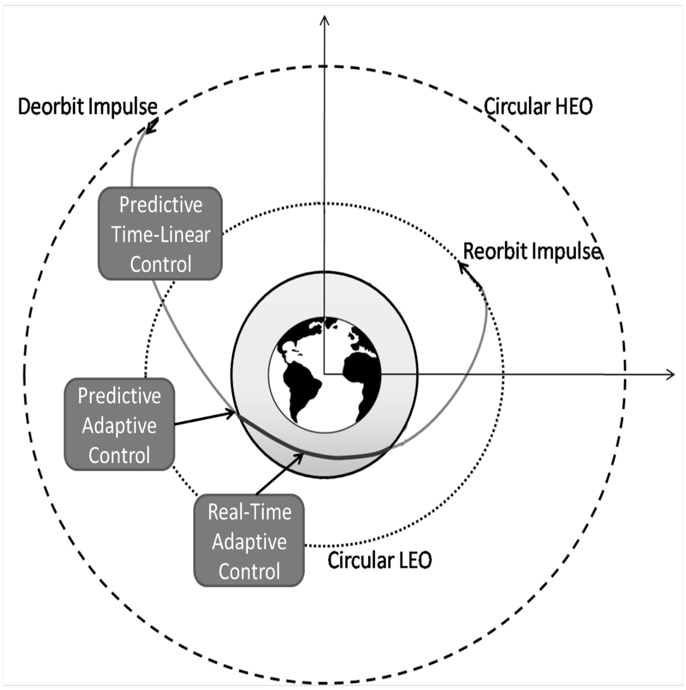

Figure 9.3: Timeline for the Mission

10

Conclusions

The present work deals with optimal aeroassisted orbital transfer from a HEO to a LEO where the part of the trajectory inside the planet's atmosphere is considered for optimization. The solution of the 2PBVP developed from the Euler-Lagrange equations has proven to be beneficial over the one presented in [9] in terms of the magnitude of maximum control input, magnitude of total control power, maximum heating rate and ease of implementation of the optimal control law. Such a control law was observed to be linear in time. Upon further study, it was concluded that a time-linear control law can be obtained for the case with free exit velocity provided the reentry conditions are in a specific ratio. Additionally, an empirical relationship was obtained to derive this control law in terms of the reentry conditions so as to avoid solving the computationally expensive two-point boundary value problems. An approximate closed-form solution for the state equations with a time-linear control law was derived and was found to be closer to the numerical solution.

It is likely that, occasionally the AOT vehicle might approach the planet's atmosphere with a different reentry condition instead of the expected one. In such cases, it is important to compensate for the initial perturbation by applying a higher control input. In order to achieve this, a terminal time LQR and an infinite time LQR were implemented. The terminal time LQR was observed to provide better compensation for the initial perturbation as compared to the infinite time LQR but requires a higher magnitude of control input and also experiences greater heating rate which are undesirable.

Alternatively, a novel method called the predictive time-linear control was suggested to compensate the initial perturbation at reentry by adjusting the initial control input (a), slope of the control input with respect to time (b) and terminal time (t'_f) for a time-linear control law where the initial perturbations are known a priori. This predictive time-linear control profile was observed to be very close to the optimal solution for the same terminal time which would imply that the predictive time-linear control is a near optimal method.An analysis was done on the variation of a, b and t'_f with respect to perturbed reentry conditions.The predictive time-linear controller is shown to adjust a, b and t'_f not only with respect to initial perturbations but even for a change in the ballistic parameter.

The predictive time-line control cannot be applied to adapt to real time changes in the ballistic parameter, especially if it is stochastic in nature. In order to be able to reach the desired exit conditions a robust feedback controller is designed and shown to compensate upto $\pm 20\%$ change in the ballistic parameter.The performance of the robust feedback controller is compared to that of a terminal time LQR in compensating for the stochastic nature of the ballistic parameter and the robust feedback controller is shown to exhibit better performance.

Alternatively, an adaptive control methodology is formulated and implemented to compensate for the uncertainty in ballistic parameter. This methodology is proven to make the system asymptotically stable and has provided satisfactory performance when applied to the AOT vehicle. The adaptive control law obtained is shown to have much less chattering as compared to that of the robust feedback controller for the same performance reducing the overall control effort required.

References

[1] G. C. Walberg, "Survey of aeroassisted orbit transfer," *AIAA Journal of Spacecraft*, vol. 22, no. 1, pp. 3–18, 1985. 4, 6, 9

[2] A.Miele and W.Y.Lee, "Optimal trajectories for hypervelocity flight," *American Control Conference, 1989*, pp. 2017–2023, 1989. 10

[3] M. Kumar and A. Tewari, "Trajectory and attitude simulation for mars aerocapture and aerobraking," *AIAA Journal of Spacecraft and Rockets*, vol. 43, no. 3, pp. 585–593, 2006. 10

[4] M. Kumar and A.Tewari, "Trajectory and attitude simulation for aerocapture and aerobraking," *AIAA Journal of Spacecraft and Rockets*, vol. 42, no. 4, pp. 684–693, 2005. 10

[5] A. V. Rao, A. E. Scherich, S. Cox, and T. E. Mosher, "A concept for operationality responsive space mission planning using aeroassisted orbital transfer," *AIAA 6th Responsive Space conference*, 2008. 11

[6] H. Takano and Y. Baba, "A note on the optimal aotv return," *IEEE Proceedings of the 41st SICE Annual Conference*, 2002. 11

[7] C. Gogu, T. Matsumura, R. T. Haftka, and A. V. Rao, "Aeroassisted orbital transfer trajectory optimization considering thermal protection system mass," *AIAA Journal of Guidance, Control and Dynamics*, vol. 32, no. 3, pp. 927–938, 2009. 11

[8] W. Loh, *Re-entry and Planetary Entry Physics and Technology-I/Dynamics, Physics, Radiation, Heat Transfer and Ablation.* Springer-Verlag, 1968. 11, 32

[9] D. Mishne, M. Idan, and Y. Laufer, "Approximate optimal planar guidance of an aeroassisted space vehicle," *AIAA Journal of Guidance, Control and Dynamics*, vol. 20, no. 4, pp. 780–789, 1997. x, 12, 25, 26, 27, 28, 29, 90

[10] T. Guo, D. Liu, and Q. Xia, "Novel aeroassisted orbital transfer optimal guidance algorithm for reentry vehicle," *IEEE 3rd International Conference on Advanced Computer Theory and Engineering(ICACTE)*, 2010. 12, 19

[11] Z. Shen and P. Lu, "Onboard generation of three-dimensional constrained entry trajectories," *AIAA Journal of Guidance, Control and Dynamics*, vol. 26, no. 1, pp. 111–121, 2003. 12, 19

[12] S. Naidu, J. L. Hibley, and C.D.Charalambous, "Neighboring optimal guidance for aeroassisted orbital transfer," *IEEE Transactions on Aerospace and Electronic Systems*, vol. 29, no. 3, pp. 656–665, 1993. 12, 45

[13] A. Tewari, *Atmospheric and Space Flight Dynamics.* Birkhauser, 2006. 16, 18

[14] A. E. B. Jr. and Y.-C. Ho, *Applied Optimal Control - Optimization, Estimation and Control*, 2nd ed. 270 Madison Avenue, New York: Taylor and Francis, 1975. 21

[15] A.Tewari, *Advanced Control of Aircraft, Spacecraft and Rockets.* John Wiley and Sons, 2011. 21

[16] L. F. Shampine, I. Gladwell, and S. Thompson, *Solving ODEs with MATLAB.* Cambridge University Press, 2003. 26

[17] A. Tewari, *Modern Control Design with MATLAB and Simulink.* John Wiley and Sons, 2002. 47, 50, 51

[18] K. J. Astrom and B. Wittenmark, *Adaptive Control.* Addison-Wesley Publishing Company, Inc., 1995. 79, 81

[19] A. Ilchmann, D. H. Owens, and D. Pratzel-Wolters, "Sufficient conditions for stability of linear time-varying systems," *Systems & Control Letters*, vol. 9, pp. 157–163, 1987. 79